Cell

Matrix Elasticity Directs Stem Cell Lineage Specification

Adam J. Engler,[1,2] Shamik Sen,[1,2] H. Lee Sweeney,[1] and Dennis E. Discher[1,2,3,4,*]
[1] Pennsylvania Muscle Institute
[2] School of Engineering and Applied Science
[3] Cell & Molecular Biology Graduate Group
[4] Physics Graduate Group
University of Pennsylvania, Philadelphia, PA 19104, USA
*Contact: discher@seas.upenn.edu
DOI 10.1016/j.cell.2006.06.044

SUMMARY

Microenvironments appear important in stem cell lineage specification but can be difficult to adequately characterize or control with soft tissues. Naive mesenchymal stem cells (MSCs) are shown here to specify lineage and commit to phenotypes with extreme sensitivity to tissue-level elasticity. Soft matrices that mimic brain are neurogenic, stiffer matrices that mimic muscle are myogenic, and comparatively rigid matrices that mimic collagenous bone prove osteogenic. During the initial week in culture, reprogramming of these lineages is possible with addition of soluble induction factors, but after several weeks in culture, the cells commit to the lineage specified by matrix elasticity, consistent with the elasticity-insensitive commitment of differentiated cell types. Inhibition of nonmuscle myosin II blocks all elasticity-directed lineage specification–without strongly perturbing many other aspects of cell function and shape. The results have significant implications for understanding physical effects of the in vivo microenvironment and also for therapeutic uses of stem cells.

INTRODUCTION

Adult stem cells, as part of normal regenerative processes, are believed to egress and circulate away from their niche (Katayama et al., 2006), and then engraft and differentiate within a range of tissue microenvironments. The tissue or matrix microenvironments can be as physically diverse as those of brain, muscle, and bone precursor osteoid (respectively, Flanagan et al. 2002; Georges et al., 2006; Kondo et al., 2005, Engler et al., 2004a; Ferrari et al., 1998; Andrades et al., 2001; Holmbeck et al., 1999; Morinobu et al., 2003). Mesenchymal stem cells (MSCs) are marrow-derived and have indeed been reported to differentiate into various anchorage-dependent cell types, including neurons, myoblasts, and osteoblasts (respectively, [Deng et al., 2005; Hofstetter et al., 2002; Kondo et al., 2005], [Pittenger et al., 1999], and [McBeath et al., 2004; Pittenger et al., 1999]). For differentiated cells such as fibroblasts, it is well known that responses to the typical soluble inducers such as growth factors couple to matrix anchorage (Nakagawa et al., 1989). However, with naive stem cells, direct effects of matrix physical attributes such as matrix stiffness have yet to be examined.

Differentiated cells ranging from neurons to osteoblasts adhere, contract, and crawl not only within soft tissues such as that of the brain or on top of crosslinked collagen ''osteoids'' in remodeling bone but also in vitro on collagen-coated acrylamide gels and glass (Figure 1A). Such a wide variation in matrix stiffness for differentiated cells is known to influence focal-adhesion structure and the cytoskeleton (Bershadsky et al., 2003; Cukierman et al., 2001; Discher et al., 2005; Engler et al., 2004a; Lo et al., 2000; Pelham and Wang, 1997). Past results with cells committed to a particular lineage, especially fibroblasts, on floating collagen gels and wrinkling-silicone sheets also suggest some responsiveness to the physical state of the matrix (Hinz et al., 2001; Nakagawa et al., 1989; Tomasek et al., 2002; Wozniak et al., 2003), but gel porosity and film topography complicate identification of possible contributions of substrate stiffness. In contrast, tissue-level matrix stiffness is distinct and shown here in sparse cultures to exert very strong effects on the lineage specification and commitment of naive MSCs, as evident in cell morphology, transcript profiles, marker proteins, and the stability of responses.

How might MSCs ''feel'' or sense matrix elasticity and transduce that information into morphological changes and lineage specification? At the molecular scale, matrix sensing first requires the ability to pull against the matrix and, secondly, requires a cellular mechano-transducer(s) to generate signals based on the force that the cell must generate to deform the matrix. Of the cell's cytoskeletal motors, one or all of the nonmuscle myosin II isoforms (NMM IIA, B, and C [Kim et al., 2005]) are candidates, as they are implicated in tensioning cortical actin structures

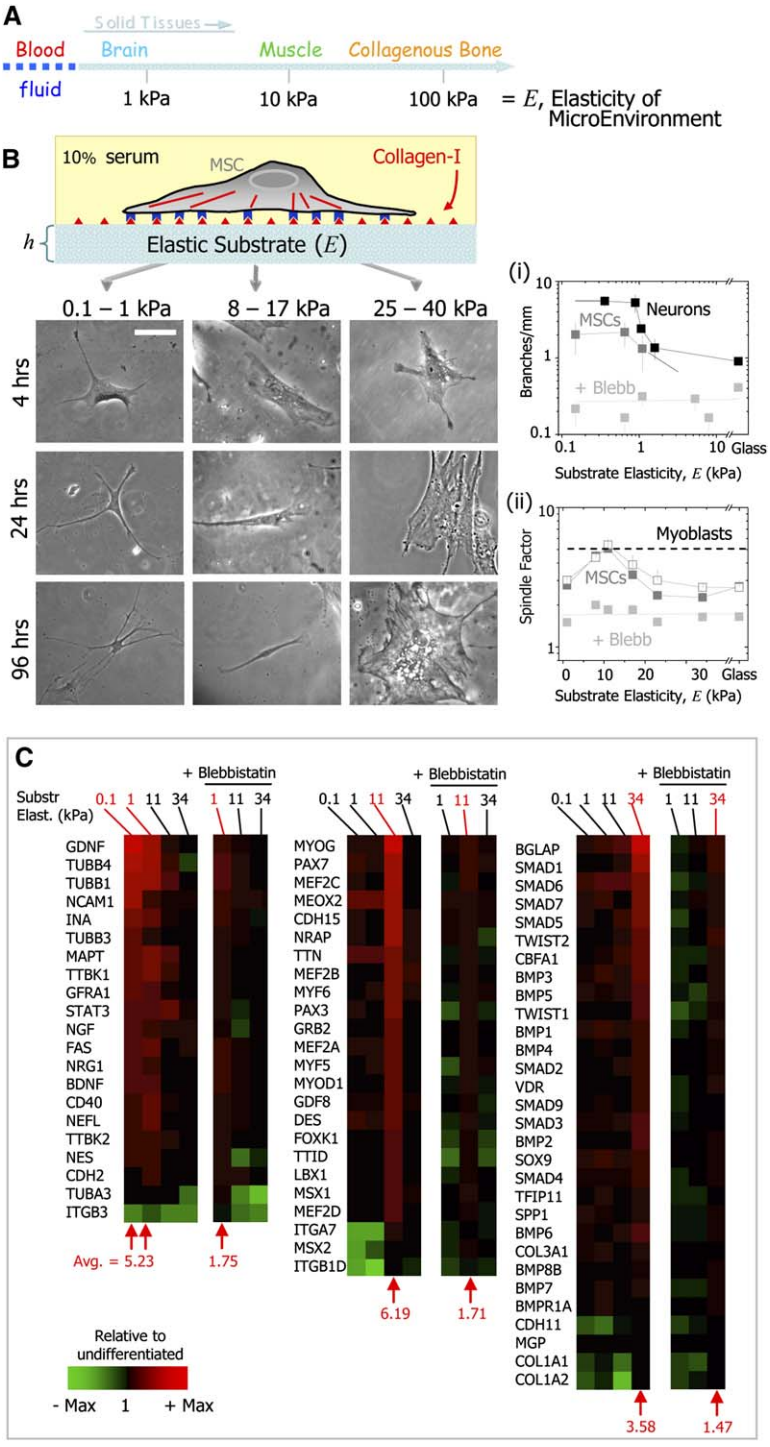

Figure 1. Tissue Elasticity and Differentiation of Naive MSCs

(A) Solid tissues exhibit a range of stiffness, as measured by the elastic modulus, *E*.

(B) The in vitro gel system allows for control of *E* through crosslinking, control of cell adhesion by covalent attachment of collagen-I, and control of thickness, *h*. Naive MSCs of a standard expression phenotype (Table S1) are initially small and round but develop increasingly branched, spindle, or polygonal shapes when grown on matrices respectively in the range typical of $\sim E_{brain}$ (0.1–1 kPa), $\sim E_{muscle}$ (8–17 kPa), or stiff crosslinked-collagen matrices (25–40 kPa). Scale bar is 20 μm. Inset graphs quantify the morphological changes (mean ± SEM) versus stiffness, *E*: shown are (*i*) cell branching per length of primary mouse neurons (Flanagan et al., 2002), MSCs, and blebbistatin-treated MSCs and (*ii*) spindle morphology of MSCs, blebbistatin-treated MSCs, and mitomycin-C treated MSCs (open squares) compared to C2C12 myoblasts (dashed line) (Engler et al., 2004a).

(C) Microarray profiling of MSC transcripts in cells cultured on 0.1, 1, 11, or 34 kPa matrices with or without blebbistatin treatment. Results are normalized to actin levels and then normalized again to expression in naive MSCs, yielding the fold increase at the bottom of each array. Neurogenic markers (left) are clearly highest on 0.1–1 kPa gels, while myogenic markers (center) are highest on 11 kPa gels and osteogenic markers (right) are highest on 34 kPa gels. Blebbistatin blocks such specification (<2-fold different from naive MSCs).

(McBeath et al., 2004; Wang et al., 2002). These actin structures are in turn linked to focal adhesions that provide the pathway of force transmission from inside the cell to the elastic matrix (Beningo et al., 2001; Tamada et al., 2004) and associated with the focal-adhesion complexes are a number of well-known signaling molecules that are well-placed to act as the mechano-transducers (Bershadsky et al., 2003; Alenghat and Ingber, 2002). With MSCs here, we demonstrate that one or all of the NMM IIA–C are likely to be involved in the matrix-elasticity sensing that drives lineage specification.

The resistance that a cell feels when it deforms the ECM is measured by the elastic constant, *E*, of the matrix or microenvironment. For microenvironments of relevance here,

that of the brain (Flanagan et al., 2002) is considerably softer than muscle (Engler et al., 2004a), and muscle is softer than collagenous osteoid precursors of bone (measured here). The wide range of microenvironment elasticity highlighted in Figure 1A is central, we show, to predicting specification of MSCs. Matrix elasticity is mimicked in vitro here with inert polyacrylamide gels in which the concentration of bis-acrylamide crosslinking sets the elasticity (Pelham and Wang, 1997), and adhesion is provided by coating the gels with collagen I, which is known to support myogenic and osteogenic differentiation (Engler et al., 2004a; Garcia and Reyes, 2005). Using this well-defined, elastically tunable gel system (Figure 1B), as opposed to wrinkling films or degrading collagen gels (Hinz et al., 2001; Wozniak et al., 2003), we provide the first evidence with sparse cultures of MSCs that matrix can specify lineage toward neurons, myoblasts, and osteoblasts—all in identical serum conditions. We document the matrix regulation of key lineage markers and myosins, including NMM IIs, which—when inhibited with blebbistatin (Straight et al., 2003)—blocks differentiation. We also show that soluble induction factors tend to be less selective than matrix stiffness in driving specification, and cannot reprogram MSCs that are precommitted for weeks on a given matrix. Finally, by controlling gel thickness, h, we establish how far stem cells can feel and thus physically define their microenvironment.

RESULTS

Cell Morphology Suggests Lineage Specification Is Directed by Matrix Stiffness and Dependent on Nonmuscle Myosin II

On soft, collagen-coated gels that mimic brain elasticity ($E_{brain} \sim 0.1–1$ kPa) (Flanagan et al., 2002), the vast majority of MSCs adhere, spread, and exhibit an increasingly branched, filopodia-rich morphology (Figure 1B). Branching densities after 1 week in culture approach those of primary neurons on matrigel-coated gels (Flanagan et al., 2002), and the dynamics of outward extension with branching is clearly opposite to DMSO-induced retraction of the cell body that can leave pseudoextensions behind (Neuhuber et al., 2004). MSCs on 10-fold stiffer matrices that mimic striated muscle elasticity ($E_{muscle} \sim 8–17$ kPa) lead to spindle-shaped cells similar in shape to C2C12 myoblasts (Engler et al., 2004a). Stiffer matrices (25–40 kPa) that we show below mimic the crosslinked collagen of osteoids (Garcia and Reyes, 2005; Kong et al., 2005) yield polygonal MSCs similar in morphology to osteoblasts. Analyses of cell morphologies (Figure 1B; plots i and ii) show that matrix-dependent shape variations of MSCs are similar to differentiated cells. It is important to also note in these plots and elsewhere below that the results with stiff acrylamide gels extrapolate to those with collagen-coated, rigid glass; this is expected if substrate elasticity is a key variable of importance. Furthermore, since the inhibition of proliferation by mitomycin-C (open squares, Figure 1B; plot ii) has little impact on average cell shape, the morphology results are consistent with lineage development being a population-level response to substrate elasticity.

As introduced above, nonmuscle myosin II is likely to be involved in exerting force through focal adhesions in mechanisms of sensing matrix elasticity. All of the NMM II isoforms are inhibited by blebbistatin, which does not inhibit any other myosin found in MSCs (see below), other than myosin VI (Limouze et al., 2004). Addition of blebbistatin during plating blocks branching, elongation, and spreading of MSCs on any substrate (Figure 1B; plots); however, addition of blebbistatin 24 hr postplating does not significantly reverse cell shape or spreading on E_{muscle} gels after the cells have already spread and adopted a spindle morphology (e.g., 24 hr per Figure 1B). Less specific and less potent myosin inhibitors such as BDM (at ~mM concentrations) are already known to block neuronal motility as well as the sensitivity of differentiated cells to substrate elasticity (Pelham and Wang, 1997), but blebbistatin is far more selective and potent (Straight et al., 2003). It inhibits actin activation of NMM II ATPase activity (at ~μM concentrations) and blocks migration and cytokinesis in vertebrate cells without affecting MLCK. Crystal structures show inhibition of actin-activated ATPase activity by blebbistatin (Allingham et al., 2005) requires a specific alanine (or serine) residue that is found only in class II and VI myosins (Limouze et al., 2004; Straight et al., 2003). We confirm below that MSCs express the three NMM IIs and myosin VI, but we implicate NMM IIs and the cytoskeleton as critical to differentiation.

To reinforce this conclusion and to rule out a role for myosin VI in matrix sensing, we repeated the above experiments with the myosin light chain kinase (MLCK) inhibitor, ML7 (Dhawan and Helfman, 2004). Of the myosins found in MSCs thusfar (see below), regulatory light chain phosphorylation via MLCK is only used to activate the NMM IIs. ML7 will block activation of these as well as smooth muscle myosin isoforms but will not affect activation of any other myosins in MSCs. Results with ML7 prove below to be identical to those seen with blebbistatin, and so NMM II activity appears to be necessary for matrix elasticity-driven lineage specification.

RNA Profiles Indicate Lineage Specification on Matrices of Tissue-like Stiffness

Transcriptional profiles of neurogenic, myogenic, and osteogenic markers—from early commitment markers through mid/late development markers—prove consistent with indications from morphology. On the softest gels, MSCs show the greatest expression of neurogenic transcripts (Figure 1C, left column; Table S3). Neuron-specific cytoskeletal markers such as nestin, an early commitment marker, and β3 tubulin, expressed in immature neurons, as well as the mature marker neurofilament light chain (NFL) (Lariviere and Julien, 2004) and the early/midadhesion protein NCAM (Rutishauser, 1984), are all upregulated. In terms of a simple average across various key

neurogenic transcripts, upregulation on the softest gels is 5-fold above early passage MSCs. On moderately stiff matrices near E_{muscle} (11 kPa), MSCs express 6-fold more myogenic message, with clear upregulation of early to late transcriptional proteins such as Pax activators and myogenic factors (e.g., MyoD); comparisons of expression levels to committed muscle cells are also provided below. On the stiffest matrices (34 kPa), MSCs express 4-fold greater osteogenic message, upregulating osteocalcin and the early transcriptional factor CBFα1 (middle and right column, respectively). Importantly, transcriptional profiles of early versus late MSCs (up to passage 12) do not differ significantly (Table S1), even though population expansion has been suggested by others to dramatically alter MSCs (Maitra et al., 2005). However, lineage specification on each matrix is clearly blebbistatin sensitive (Figure 1C + blebbistatin).

A number of terminal differentiation markers such as lineage specific integrins (α3, α7, and β1D) and morphogenetic proteins are not upregulated relative to naive MSCs. However, these are generally not expressed until later development, e.g., cell fusion into myotubes is required for β1D expression. Matrix stiffness undoubtedly couples to cell density for fusion and synaptogenesis as well as other noncollagenous ECM components and soluble factors (see below).

Clarifying Neuro-Induction and Osteogenic Microenvironments

The results above and that follow below provide insight into the NMM II-based contractility and considerable sensitivity of stem cells to mechanical microenvironment, which are important issues in and of themselves, but the results also bring to the fore several questions in the literature regarding induction strategies and the physical nature of in vivo microenvironments. For example, uncertainty exists regarding the inducibility of stem cells toward neurogenic lineages. Soluble agonists such as retinoic acid and dimethylsulfoxide (DMSO) have been reported to induce reversible branching in stem cells (Dinsmore et al., 1996; Woodbury et al., 2002), but DMSO also causes fibroblasts to appear "branched," and this appears due to cytoskeletal disruption with centripetal retraction of the cell body that leaves extensions attached (Neuhuber et al., 2004).

The time series of images in Figure 1B shows outwardly branching MSCs on the softest gels (0.1–1 kPa) which, in immunofluorescence (Figure 2A), also show expression and branch localization of neuron-specific β3 tubulin and neurofilament heavy chain (NFH and its phosphoform, P-NFH). The latter are widely recognized as late neuronal markers (Lariviere and Julien, 2004). Indeed, both MSCs and primary neurons (Flanagan et al., 2002) spread and branch with time on the softest matrices (Figure 2B), unlike fibroblasts that do not branch or express neurogenic proteins. Similarly, on myogenic matrices, both MSCs and myoblasts spread and become spindle shaped with time, unlike fibroblasts (Figure S1A). Intensity analyses of immunofluorescent images (e.g., Figures 2A and 2C) as well as Western blots (Figure 2C; inset) confirm that only cells on the softest matrices express protein markers for neuronal commitment (nestin), immature neurons (β3 tubulin), mid/late neurons (microtubule associated protein 2; MAP2), and even mature neurons (NFL, NFH, and P-NFH). These findings clearly agree with neurogenesis of MSCs, as seen in more complex microenvironments, especially the brain (Kondo et al., 2005; Wislet-Gendebien et al., 2005).

Uncertainty also exists in the literature regarding the compliance and thickness of osteoid. This crosslinked collagen precursor to bone is secreted by osteoblasts and reportedly is the matrix upon which MSCs undergo a transition to preosteoblasts (Figure 2D) (Andrades et al., 2001; Morinobu et al., 2003; Raisz, 1999), before the matrix calcificies over week(s) (Rattner et al., 2000) to rigid bone ($\sim 10^6$ kPa). We have made the first measurements here of the compliance and thickness of the osteocalcin-rich osteoid matrix (Figure 2E) that surrounds osteoblasts in culture (see AFM in Experimental Procedures). The matrix is 350 $\pm$ 100 nm thick (Figure 2F) and has a stiffness, $E_{osteoid} \sim 27 \pm 10$ kPa (Figure 2G), that is similar to a concentrated collagen gel (Roeder et al., 2002). Osteoid thus possesses stiffness in the same range that we find MSCs take on the shape and expression profiles of an osteogenic lineage (25–40 kPa in Figures 1B and 1C).

Cytoskeletal Markers and Transcription Factors also Indicate Lineage Specification

Immunostaining of cytoskeletal markers and transcription factors across the range of matrix stiffnesses (Figure 3A) proves consistent with the lineage profiling of Figure 1. On the softest, neurogenic matrices, a majority of cells express β3 tubulin, which, along with P-NFH and NFH, is visible in long, branched extensions but is poorly expressed, if at all, in cells on stiffer gels (Figure 2C). On moderately stiff, myogenic matrices, MSCs upregulate the transcription factor MyoD1, localizing it to the nucleus (large arrow; Figure 3A). Compared with C2C12 myoblasts, transcript levels (Figure 3B; Table S3) as well as fluorescence intensity analyses (Figure 3C) indicate about 50% relative expression levels after 1 week on the myogenic matrix; MSCs on softer and stiffer matrices do not express significant MyoD1 or other muscle markers (e.g., titin, pax-3,7, and myogenin). On the stiffest, osteogenic matrices, MSCs upregulate the transcription factor CBFα1 (Figure 3A; open arrow), which is a crucial early marker of osteogenesis (Gilbert et al., 2002). Compared with hFOB osteoblasts, transcript levels (Figure 3B; Table S3) as well as fluorescence intensity analyses (Figure 3C) again indicate about 50% relative expression levels after 1 week on the osteogenic matrix; MSCs on softer matrices do not express significant CBFα1 or other osteoblast markers (e.g., collagen-1s and BMPs).

Elasticity-directed marker protein expression on the various substrates is summarized in Figure 3C. A single,

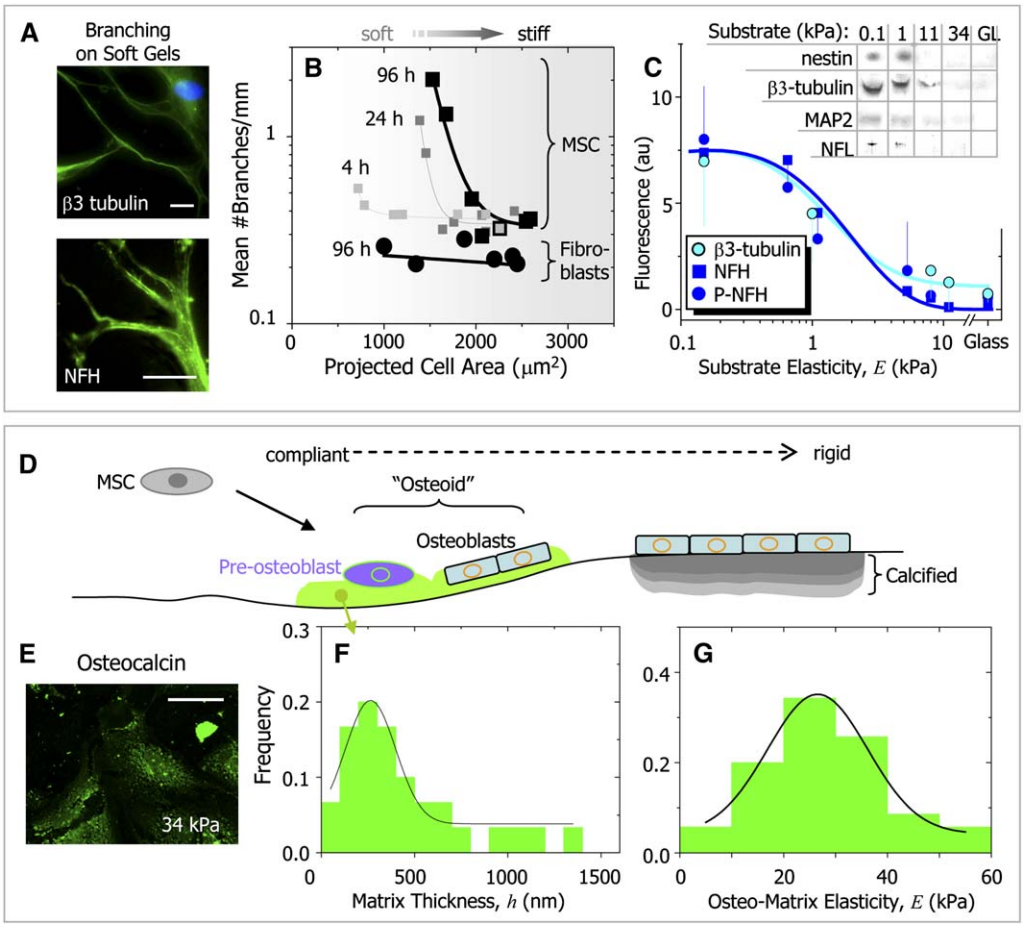

Figure 2. Neurogenic Branching and Osteogenic Microenvironments

(A) Immunofluorescence images of β3 tubulin and NFH in branched extensions of MSCs on soft matrices ($E \sim 1$ kPa). Scale bars are 5 μm.

(B) MSCs and fibroblasts on a range of elastic matrices show an increase in projected area with matrix stiffness, but only MSCs on the softest gels (with smallest areas) show an increasing number of branches per extension length with time.

(C) β3 tubulin, NFH, and P-NFH all localize to the branches of MSCs on the softest substrates with $E < 1$ kPa (mean ± SEM). Nestin, β3 tubulin, MAP2, and NFL Western blotting (inset) confirms expression only on soft gels.

(D) Schematic of the compliant, collagenous "osteoid" microenvironment (green) that MSCs encounter in initial remodeling of bone matrix (adapted from Raisz, 1999). Committed osteoblasts remodel microenvironments by secreting matrix proteins that are slowly calcified.

(E) hFOB osteoblasts secrete osteocalcin after being plated on glass. By day 7, the matrix is thick (F) and compliant with $E_{osteo} \sim 25$–40 kPa (G) based on measurements made by AFM.

nonoverlapping optimum in matrix stiffness after 1 week is seen for the specification of each of the three lineages. The intensity scale is normalized to the primary cells C2C12 and hFOB, which also show optimal matrix elasticities for expression (MyoD and CBFα1, respectively) and further exhibit an elevated baseline in expression on suboptimal matrices. In other words, primary cells appear preprogrammed to express an elevated basal level of the characteristic markers regardless of matrix. In contrast, MSCs express no significant levels of the lineage markers, except of course on the optimal matrices. Blebbistatin again blocks expression of all markers on all matrices (Figure 3C; gray curve), consistent with an inhibition of the cell's ability to feel and respond to its matrix.

Induction Media Adds to Inductive Matrix before Lineage Commitment

In culture, differentiation of MSCs is usually induced by addition of specific soluble factors, such as Dexamethasone, which can permeate cell membranes and can, in principle, directly activate lineage programs. The myoblast induction media used here (MIM, Table S2) is already known to promote myogenesis, with expression of MyoD, Myogenin, and skeletal muscle myosin heavy chain (Gang et al., 2004; Pittenger et al., 1999). Across the various elastic matrices here, MIM induces MSCs to express high basal levels of MyoD that approach the constitutive expression levels of C2C12 myoblasts (Figure 4A). A clear peak for MSC + MIM on the myogenic matrix (8–17 kPa)

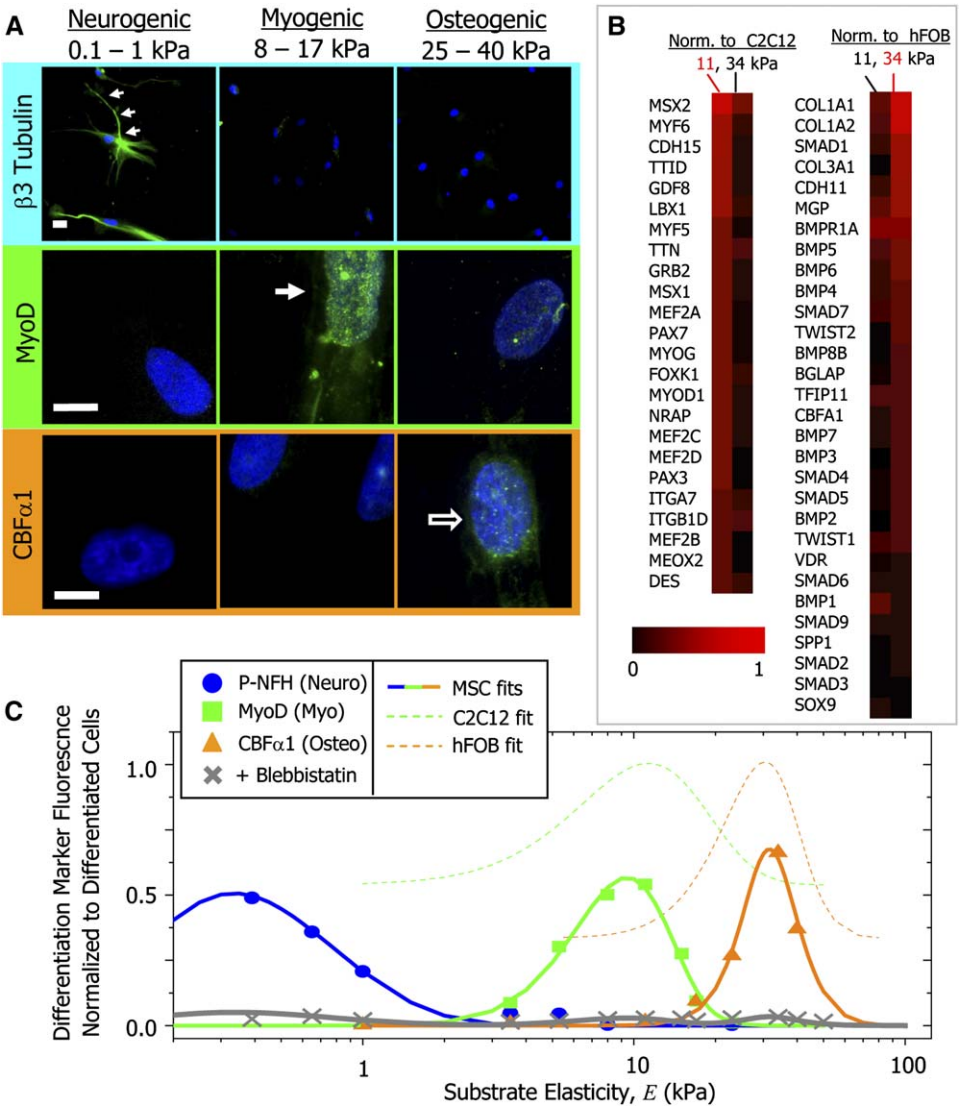

Figure 3. Protein and Transcript Profiles Are Elasticity Dependent under Identical Media Conditions

(A) The neuronal cytoskeletal marker β3 tubulin is expressed in branches (arrows) of initially naive MSCs (>75%) and only on the soft, neurogenic matrices. The muscle transcription factor MyoD1 is upregulated and nuclear localized (arrow) only in MSCs on myogenic matrices. The osteoblast transcription factor CBFα1 (arrow) is likewise expressed only on stiff, osteogenic gels. Scale bar is 5 μm.

(B) Microarray profiles of MSCs cultured on 11 or 34 kPa matrices, with expression normalized first to actin and then to expression of committed C2C12 myoblasts and hFOB osteoblasts.

(C) Fluorescent intensity of differentiation markers versus substrate elasticity reveals maximal lineage specification at the *E* typical of each tissue type. Average intensity is normalized to peak expression of control cells (C2C12 or hFOB), for which only fits to Equation S3 are shown. Blebbistatin blocks all marker expression in MSCs.

is evident and suggests a statistically similar level of lineage commitment for MSCs and C2C12 cells.

Addition of blebbistatin to persistently block NMM II activity (i.e., MIM + blebbistatin) still blocks cell spreading, but MyoD expression is found to be significantly above baseline. However, expression lacks the usual matrix-induced peak expression near E_{muscle} (Figure 4A). Thus, matrix-driven expression changes appear to depend on active NMM II, while induction media stimulates basal-level myogenesis regardless of cell shape or active NMM II. Additionally, when blebbistatin is added to MSCs that are allowed to first spread and become spindle shaped for 24 hr on E_{muscle} gels (see Figure 1B), MSCs maintain their morphology (Figure S2), but the blebbistatin suppresses MyoD expression. Subsequent washout of the drug 72 hr later allows full recovery of MyoD expression. When taken together, (1) lack of MyoD expression by spindle-shaped blebbistatin-treated MSCs, (2) induced

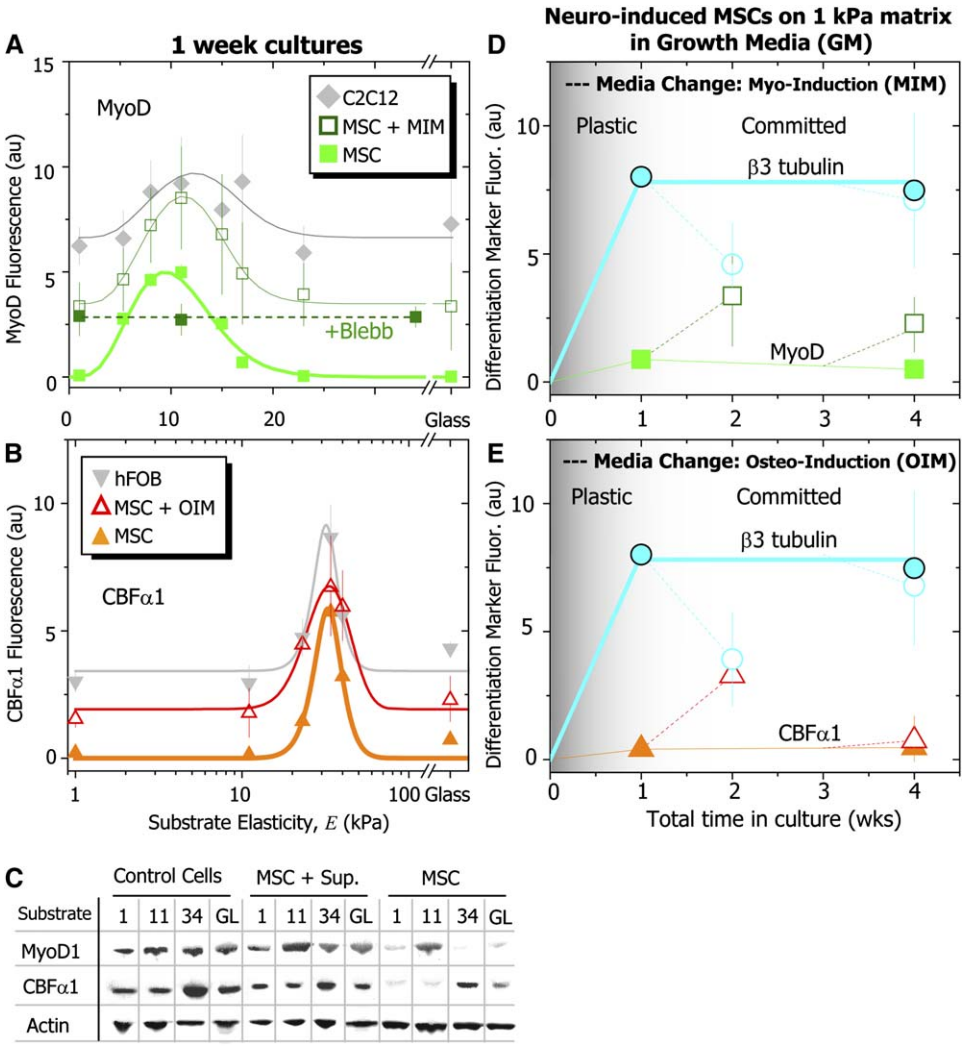

Figure 4. Induction Media and Matrix Reveal Synergy as well as Lineage Plasticity and Eventual Commitment

(A and B) After 1 week in culture in standard MSC growth media, fluorescent intensities of MyoD1 and CBFα1 in MSCs reveal little to no expression except at peaks near E_{muscle} and E_{osteo}, respectively. When myogenic or osteogenic induction media (MIM or OIM) is added, MyoD1 or CBFα1 expression occurs on all substrates, with peak expression at levels near those of control cells, indicating a synergy of matrix and media induction. When cultured in both MIM and blebbistatin (filled symbol and dashed line), MSCs also express a constant level of MyoD. Curve fits throughout use Equation S3.

(C) Western blots confirm lineage specification with matrix or supplemented media alone: when normalized to actin, CBFα1, and MyoD expression reach control levels only when both matrix stiffness and media are conducive for specification.

(D and E) MSCs plated on neurogenic matrices in standard growth media were cultured for 1 or 3 weeks prior to having their media changed to MIM or OIM for an additional week (open data points). After mixed induction for 1 week + 1 week, MSC expression of β3 tubulin is seen to decrease while MyoD1 or CBFα1 expression increases, thus creating *trans*-differentiated cell types when compared to cultures in normal growth media (closed data points). However, after 3 weeks of matrix induction, MSCs become committed and unperturbed by 1 week in *trans*-induction media. Cells remain branched and express the same high levels of β3 tubulin with little to no significant expression of MyoD or CBFα1. Fluorescence intensities (mean ± SEM) were measured for dual-labeled cells.

expression in MIM of unspread cells, and also (3) MIM-induced MyoD expression on "incorrect" matrices (e.g., MSC + MIM on 1 kPa or 34 kPa gels) all imply that active NMM II is indeed important to lineage specification independent of cell shape. It is also clear, however, that on ECM with the "correct" elasticity, active NMM IIs, and soluble induction factors synergistically combine for more complete myogenesis, as calibrated against committed cells (i.e., C2C12).

Similar results as above are found with a standard osteoblast induction media (OIM), which is known to promote cytoskeletal rearrangement and alkaline phosphatase production (Jaiswal et al., 1997; McBeath et al., 2004). Increased basal expression of CBFα1 occurs on all

substrates, and there is still a clear optimum for lineage specification on the stiffest, osteogenic gels (Figure 4B). The quantitative immunofluorescence assessments above are confirmed by Western blots and clearly highlight the precommitted nature of C2C12 and hFOB "control cells" as well as both the constitutive and additive effects of induction media on MSCs (Figure 4C).

The results above indicate that cells grown on a matrix that is, for example, neurogenic due to its softness (1 kPa), can be induced by soluble factors (MIM or OIM) to also express myogenic or osteogenic factors yielding a "mixed MSC phenotype." To assess commitment due to matrix alone, MSCs were preplated in standard growth media for either 1 or 3 weeks on the soft neurogenic gels and then switched to the different induction media. Without the added induction media, cells stably express the neurogenic marker β3 tubulin at a constant level from 1 to 4 weeks (Figures 4B and 4D; closed points). However, when either MIM or OIM is added after 1 week, a further week of culture reduces β3 tubulin levels by about half and increases negligible MyoD levels several-fold (Figures 4B and 4D; open points). These "mixed phenotype" MSCs display multiple lineage signals, albeit at low levels, rather than creating two MSC populations committed to different lineages in the same culture, as cells at this plating concentration are very slow to proliferate, even in growth media (McBeath et al., 2004). In contrast, when MSCs are preincubated for 3 weeks on neurogenic matrices before switching media for a final week, MSCs are less plastic and more firmly committed to their matrix-defined lineage: high levels of β3 tubulin remain statistically the same, and CBFα1 is essentially undetectable. Similar results are also observed for matrix changes where MSCs, replated from stiff to soft matrices, maintain their original specification when given sufficient incubation time (not shown). Slight perturbations under delayed mixed induction might be real (e.g., MyoD upregulation in Figure 4D), since plasticity of "differentiated" cell types has been demonstrated in various systems with (a) chemical agonists that *trans*-differentiate myotubes (Rosania et al., 2000), (b) transfected transcription regulators that *trans*-differentiate fibroblasts to myoblasts (Davis et al., 1987), and (c) classical growth factor pathways that *trans*-differentiate myotubes to osteocytes (Katagiri et al., 1994).

Myosins in MSCs Couple Expression to Matrix Stiffness and Reveal a Key Role for NMM IIs

Forces generated and/or imposed on the cell's actin cytoskeleton have been postulated to influence differentiation (Engler et al., 2004a; Hinz et al., 2001; McBeath et al., 2004), but no past reports have hinted at strong, tissue-directed feedback of microenvironment elasticity on myosin expression or stem cell lineage specification. Cellular tension must be modulated by matrix stiffness, with force transmission occurring via focal adhesions. As described in the introduction and supported by the blebbistatin and ML7 results above, the likely generators of force are the nonmuscle myosin II isoforms. We indeed find that these and a number of myosin transcripts are not only expressed in naive MSC but also upregulated on stiffer gels (11 and 34 kPa) when compared to softer matrices (Figure 5A; left). Western blots and immunofluorescent imaging both confirm array results and show that NMM IIB is up more than 2-fold relative to myosin levels before differentiation (Figures 5B and 5C) on stiff matrices but is downregulated on the softest substrates. It is also found that induction media has comparatively little effect on these stiffness-responsive expression profiles (Figure 5C). The kinetics of NMM IIB imply that it generates higher force than NMM IIA (Rosenfeld et al., 2003) since it spends a greater amount of time strongly attached to actin. We therefore speculate that as matrix stiffness increases, the cell alters its nonmuscle myosin expression in order to generate greater forces on its actin cytoskeleton, which would be necessary to deform a stiffer matrix.

Select myosin genes appear more matrix sensitive than others based on microarray data clustered by RNA variation (Var) (Figure 5A; left). Western blots confirm the variation; NMM IIB expression is more sensitive to matrix elasticity than NMM IIA expression (Figure 5B). The blots also confirm (1) myogenic commitment with requisite upregulation of both MyoD and the intermediate filament protein desmin (Weitzer et al., 1995) and (2) osteogenic commitment with CBFα1. Immunofluorescence images of NMM IIA not only reinforce microarray and blot results but further reveal changes in myosin organization (Figure 5C; inset images). On soft matrices, NMM II staining is diffuse. On moderately stiff matrices, myosin striations emerge that have an appearance previously described as premyofibrillar structures in committed myoblasts (Sanger et al., 2002). Spacing between these nascent striations is the same for MSCs and age-matched C2C12 myocytes (1.0 ± 0.3 μm), and while these striations are lost on the stiffest matrices where stress fibers predominate, NMM II striation appears consistent with nonmuscle myosin organization (Verkhovsky et al., 1995). However, the striation period is clearly smaller than the spacing set by myogenic molecular "rulers" such as titin (TTN in Figure 3B) (Sanger et al., 2002), indicating that MSCs have not assembled mature myofibrils after a week in culture. This is consistent with low levels of skeletal muscle myosin transcript (MHC2A; Figure 5A) and protein (Figure S1B), emphasizing the fact that these sparse cultures of mononucleated MSCs can become committed but remain early myoblasts.

Chronic inhibition of NMM II's ATPase activity with blebbistatin (Limouze et al., 2004; Straight et al., 2003) not only inhibits morphological changes of MSCs on various matrices (Figures 1Bi and 1Bii) but also reduces transcripts levels for NMM IIA (to 50%), IIB (to 8%), and IIC (to 3%) (Figure 5A; right). Importantly, myosins that are not directly affected by blebbistatin treatment changed to a lesser extent from control levels, with one-third of the panel showing no change (MYO5B, MYO1A, MLC3, and MYH3). This highlights the specificity of a key mechanosensing feedback loop between blebbistatin-inhibited activity

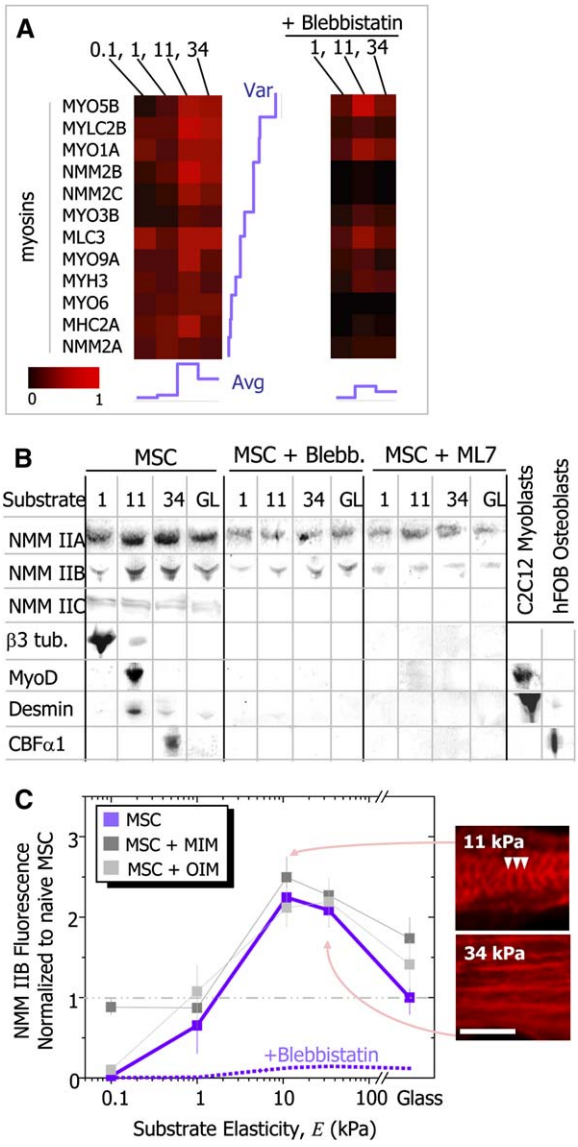

Figure 5. Multiple Myosins Are Expressed by MSCs Dependent on Matrix and Contractility

(A) A range of myosin transcripts show graded sensitivity to stiffness (Var) and an overall average expression (Avg) that is upregulated for MSCs on stiffer matrices. Blebbistatin downregulates many myosin transcripts, especially those for NMM IIB, IIC, and myosin VI, which are directly inhibited.

(B) Immunoblots show large variations with substrate stiffness in NMM IIB, C, and various differentiation markers: neurogenic (β3 tubulin), myogenic (MyoD and Desmin), and osteogenic markers (CBFα1). These also show sensitivity to blebbistatin and ML7.

(C) Immunofluorescence of NMM IIB (mean ± SEM) shows similar stiffness sensitivity and does not change with induction media (i.e. MIM or OIM), but blebbistatin inhibits expression ~10-fold (dashed line) based on Western blots. Inset images of NMM II highlight organization of NMM II with striations (arrowheads) on E_{muscle} matrix (11 kPa) and stress fibers on the stiffer matrix (34 kPa). Scale bar is 5 μm.

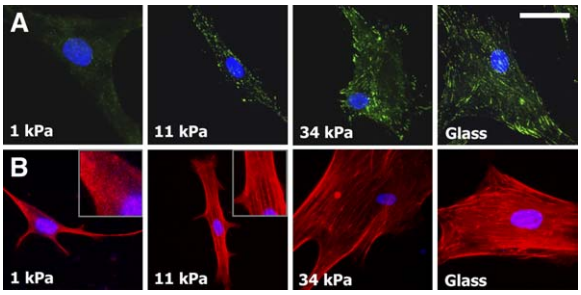

Figure 6. Adhesions Grow and Cytoskeletal Organization Increases with Substrate Stiffness

(A) Paxillin-labeled adhesions grow from undetectable diffuse "contacts" on neurogenic, soft gels (1 kPa) to punctate adhesions on stiffer, myogenic gels (11 kPa). On the stiffest, osteogenic gels (34 kPa), the adhesions are long and thin and slightly more peripheral than they appear on glass.

(B) F-actin organization shows a similar trend, from diffuse on soft gels to progressively organized on stiffer substrates (as stress fibers). Scale bar is 20 μm.

and NMM II expression. Western blots confirm similar isoform sensitivity at the protein level to blebbistatin and also to ML7, an inhibitor that also inhibits the NMM II's through its inhibition of MLCK. NMM IIA expression only slightly downregulates, while NMM IIB expression drops about 10-fold to levels comparable to MSCs on soft gels (Figures 5B and 5C), and NMM IIC is no longer detectable. The downregulation suppresses both striation and stress-fiber formation, consistent with a relaxation effect on blebbistatin-treated cells (Griffin et al., 2004) as well as the crosstalk between nonmuscle myosin II activity and morphogenetic and phenotypic specification. On soft gels, cells generally display less cytoskeletal organization (Engler et al., 2004a; Flanagan et al., 2002), as reinforced with results below. Both blebbistatin and ML7 suppress expression of key lineage markers (Figures 1C and 5B), consistent with NMM II activity, ultimately regulating lineage marker profiles in addition to its own expression.

MSC Focal Adhesions Increase with NMM II-Based Contractility and Both Increase with Matrix Stiffness

Stiff substrates promote focal adhesion growth and elongation, based on paxillin immunofluorescence (Figure 6A). Consistent with this observation, stiff substrates led to increased expression of focal adhesion components (Table S4), including nonmuscle α-actinin, filamin, talin, and focal adhesion kinase (FAK or PTK2). These results with MSCs are fully consistent with the earliest reports of the substrate-stiffness responses of differentiated cells (Pelham and Wang, 1997). We also find that MSCs feel into matrices on the length scales of their adhesions and not much deeper. This is based on the finding that a thin soft gel on glass ($h \sim 0.5$–1 μm) fosters cell spreading similar to that of cells on stiffer gels (Figure S3). Actin assembly follows the trends in adhesion assembly (Figure 6B), which

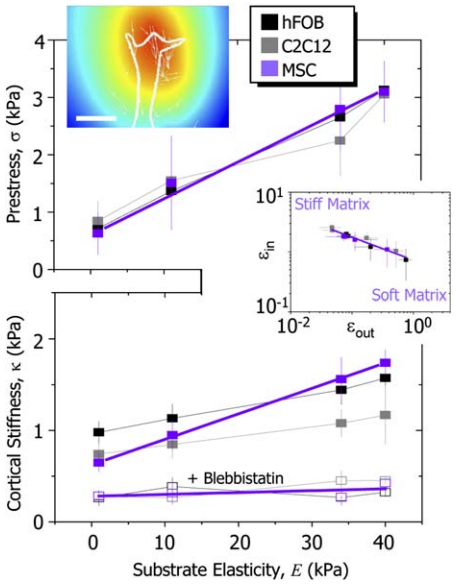

Figure 7. Stiffer Matrices Produce Stiffer and More Tense Cells

Cell prestress, σ, in both MSCs and control cell lines increases linearly with substrate elasticity, E. Inset image shows a myoblast (outlined) displacing beads embedded in the gel (white arrows) that equates to a strain field represented by the color map (red is high strain). Scale bar is 10 μm. Lower plot shows membrane cortical stiffness measured by micropipette aspiration increases with gel stiffness, but blebbistatin treatment softens all cell membranes >3-fold. Middle inset shows mean intracellular strain, ε_{in} ($\sim \sigma / \kappa$), versus the mean extracellular strain, ε_{out} ($\sim \tau / E$), fit to a power law (i.e., $\varepsilon_{in} = B\,\varepsilon_{out}^{b}$) for all cell types. The trend implies larger deformation within the cell on stiff matrices and larger deformation in the matrix on softer matrices. Results shown are Mean ± SEM.

generalizes the matrix-driven assembly of the cytoskeleton to MSCs. NMM II is already known to promote the assembly of focal adhesions (Conti et al., 2004), and so the prominent adhesions on stiffer substrates is consistent with greater activity of NMM II.

Focal adhesions provide MSCs the necessary force transmission pathways to "feel" their microenvironment through actin-myosin contractions. This pulling or contractility by cells can be measured as a mean cellular prestress, σ, that balances the traction stresses, τ, exerted on the gel by the cell (Wang et al., 2002) (Figure 7). Consistent with monotonic increases in focal adhesions versus matrix stiffness, the prestress σ for MSCs, C2C12 myoblasts, and hFOB osteoblasts all show a linear increase versus matrix stiffness (Figure 7; top). Blebbistatin prevents any of the cells from developing either a prestress σ (Griffin et al., 2004) or—as measured by a single-cell micropipette aspiration method (Figure S4)—a significant cell cortex stiffness κ on any matrix (Figure 7; bottom, open points). The simplistic measures here of cell mechanics demonstrate that stiffer matrices produce stiffer and increasingly tensed cells.

DISCUSSION

Lineage specification of naive stem cells induced by soluble stimuli has been well described (Gang et al., 2004; Jaiswal et al., 1997; McBeath et al., 2004; Pittenger et al., 1999), but the results here report a strong and previously undocumented influence of microenvironment stiffness on stem cell specification. Naive stem cells express no baseline levels of lineage-specific markers, in contrast to committed cells (myoblasts and osteoblasts in Figures 3B, 3C, 4A, and 4B), so that—against this low baseline—MSCs are seen to respond dramatically in both morphology and lineage to the matrix presented. The responses here do not include remodeling the microenvironment; for example, collagen-I production is very low in MSCs on soft matrices <11 kPa (see downregulated matrix transcripts; Figure 1C), whereas on 34 kPa matrices, MSCs appear somewhat more secretory (e.g., BMP1-5 and COL3A1), consistent with the secreting hFOB osteoblasts (Figure 2E) (Kong et al., 2005). This passive, initial response of MSCs to the microenvironment would be expected from a multipotent stem cell awaiting instruction.

MSC plasticity is evident in the initial responsiveness to conflicting signals from soft matrix and media (Figures 4D and 4E), consistent with passive responsiveness to inputs. The slow time course of true lineage commitment here contrasts with the rapid and controversial morphological changes with DMSO (Dinsmore et al., 1996; Woodbury et al., 2002). Here, MSCs spread with time, and branching increases on soft matrices (Figure 2B), indicating an active process. In contrast, fibroblasts (Figure 2B), myoblasts (Engler et al., 2004a), and osteoblasts (not shown) do not appear branched on soft substrates. The committed differentiation of the latter cell types (epigenetic) to specified lineages precludes, for example, the reprogramming of myosin levels with changes of matrix (Table S4). In comparison, MSCs prove far more responsive, and while evidence for roles of nonmuscle myosins in MSCs feeling the matrix is suggestive, more work on mechanism is clearly needed.

Possible Implications for Stem Cell Therapies

Regenerative applications of stem cells are being investigated for a number of tissues, including clinical trials for postmyocardial infarction patients (Lee et al., 2004). Efficacy appears uncertain or mixed (Murry et al., 2004), and recent findings have raised the possibility that the injured microenvironment loses compliance with fibrotic scarring, producing a noninducing environment (Berry et al., 2006) that, as we show here, stem cells cannot sufficiently remodel. The results here suggest the need for optimizing matrix elasticity to foster regeneration, which seems applicable to a number of regenerative applications of stem cells such as cardiomyoplasty, muscular dystrophy, and neuroplasty. Any starting point for such approaches must include characterization of the mechanosensitivity of the stem cell of interest to matrix elasticity.

The results of this study also suggest that "precommitting" stem cells to a specific lineage via appropriate in vitro matrix conditions might partially overcome an inappropriate in vivo microenvironment.

EXPERIMENTAL PROCEDURES

Cell Culture

Human Mesenchymal Stem Cells (MSCs; Osiris Therapeutics; Baltimore, MD), human osteoblasts (hFOBs, ATCC), primary human skin fibroblasts (1F7) (Engler et al., 2004a), and murine myoblasts (C2C12s, ATCC) were cultured in normal growth media listed in Table S2. To chemically induce differentiation, cells were placed in the appropriate induction media also listed. All cells were used at low passage numbers, were subconfluently cultured, and were plated at $\sim 10^3$ cells/cm^3 for experiments. Cells were cultured for 7 days or cultured and replated for a specified time unless otherwise noted. All chemicals were purchased from Sigma (St. Louis, MO) unless otherwise noted. To inhibit proliferation, cells were exposed to mitomycin C (10 μg/ml) for 2 hr and washed three times with media prior to plating. Blebbistatin (50 μM, EMD Biosciences), a nonmuscle myosin II inhibitor, was applied with every media change and was stable in culture media for up to 48 hr, as determined by thin-layer chromatography. Y27632 (10 μM, EMD Biosciences), a ROCK inhibitor, and ML7 (10 μM; EMD Biosciences), a myosin light chain kinase inhibitor, were also added to inhibit specification.

Substrate Preparation

Cells were plated on variably compliant polyacrylamide gels, according to a previously established protocol by Pelham and Wang (Pelham and Wang, 1997), creating gels that were ~70–100 μm thick as measured by microscopy. To produce thin gels, a protocol from Engler and coworkers was used (Engler et al., 2004b). Type 1 collagen was used at 0.25–1 μg/cm^2 (BD Biosciences), as quantified using fluorescent collagen for calibration (per Engler et al., 2004a).

AFM for Matrix Elasticity and Cell Mechanics Methods

Substrate elasticity was characterized per Engler et al. (2004b). For matrix secreted by hFOB osteoblasts, cells were plated for 7 days on glass substrates to allow matrix deposition. Samples were placed on an Asylum 1-D atomic force microscopy (AFM) (Asylum Research; Santa Barbara, CA) and indented by a pyramid-tipped probe (Veeco; Santa Barbara, CA) with a constant, k_{sp} ~60 pN/nm. Force-indentation profiles were obtained immediately adjacent to a cell, and each indentation profile was fit up to the point at which probe indentation into the secreted matrix stopped with a Hertz cone model (Rotsch et al., 1999). Details of the cell mechanics measurements can be found in the Supplemental Data.

Lineage Specification Assays

Morphological Changes and Immunofluorescence

Changes in cell shape (<4 days), especially the development of branches (Flanagan et al., 2002) or spindle-like morphologies (Engler et al., 2004a), were quantified either by the number of membrane branches per mm of cell or by a "spindle factor," the major/minor cell axis, respectively. Cells also were stained with lineage-specific antibodies: myogenesis with Myogenesis Differentiation Protein 1 (MyoD1; Chemicon) and desmin (Sigma); osteogenesis with Core Binding Factor α1 (CBFA1; Alpha Diagnostic International) and osteocalcin (EMD Biosciences); and neurogenesis with phosphorylated and dephosphorylated Neurofilament Heavy chain (NFH; Sternberger Monoclonal), Neurofilament Light chain (NFL; Sigma), nestin (BD Pharmagen), Microtubule Associated Protein 2 (MAP2; Chemicon), and β3 tubulin (Sigma) along with paxillin (Chemicon), skeletal muscle myosin heavy chain (Zymed), nonmuscle myosin IIA and IIB (Sigma), IIC (courtesy of R. Adelstein, NIH), and rhodamine-labeled phalloidin. Cells were fixed, blocked, permeabilized, and labeled with Hoechst 33342, primary and secondary antibodies, or 60 μg/ml TRITC-phalloidin.

Cell morphology and fluorescently labeled cells were examined on a TE300 inverted epifluorescent Nikon or Olympus (TIRF) microscope, imaged on a Cascade CCD camera (Photometrics), and quantified with Scion Image. Intensity analysis was displayed as the fold-change of the whole cell average above background fluorescence and staining with secondary antibodies only. For Figure 3C only, however, intensities were then normalized by the maximal expression of the positive control cell. For Figure 5C only, intensities were then normalized by the expression of initially isolated MSCs to show a change from the initial myosin level.

Western Blotting

Cells were plated on gels on 45 × 50 sq. mm coverslips to obtain enough cells for Western blotting. Cells were permeablized (1:1 of 10% SDS, 25 mM NaCl, 10 nM pepstatin, and 10 nM leupeptin in distilled water and loading buffer), boiled for 10 min, and placed in reducing PAGE (Invitrogen). Proteins were transferred onto nitrocellulose, blocked, and labeled via HRP-conjugated antibodies (Biorad). All Westerns were run in duplicate, along with an additional blot for actin and Coomassie blue staining to ensure constant protein load among samples.

Oligonucleotide Array Assays

Total RNA (3–5 μg) was obtained from MSCs cultured on gel substrates of varying stiffness, as well as C2C12 myoblasts and hFOB osteoblasts, using an ethanol-spin column extraction. Samples were labeled with an Ampolabeling Linear Polymerase Reaction kit (SuperArray Bioscience) and hybridized to custom oligonucleotide arrays. Chemiluminescent signals were detected on Biomax Film (Kodak). Arrays were first corrected for array background fluorescence and normalized to a control gene, β-actin. Data for genes indicating mesenchymal origin (Table S1) along with genes for contractile, adhesive, and activating proteins (Table S4) were displayed only as this actin-normalized value. Genes for neuro-, myo-, and osteogenesis, however, were further analyzed by either (1) comparing MSCs on gels to initially isolated MSCs (Figure 1C and Table S3; i.e., [MSC on specific gel]/[initially isolated MSC]) or (2) normalizing MSC expression on gels to control cell expression level (Figure 3B and Table S3; i.e., [MSC on specific gel]/[control cell]).

Supplemental Data

Supplemental Data include four figures, four tables, experimental procedures, and references and can be found with this article online at http://www.cell.com/cgi/content/full/126/4/677/DC1/.

ACKNOWLEDGMENTS

We gratefully acknowledge Drs. Jean and Joe Sanger, Dr. Paul Janmey, Dr. Jonathan Raper, Dr. Masaki Noda, Dr. Louis, and Dr. Robert Adelstein for reagents and discussions. Support was provided by grants from NIAMS (H.L.S. and D.D.), NHLBI and NIBIB (D.D.), MDA (H.L.S. and D.D.), NSF (D.D.), NSF-MRSEC, and the Ashton Foundation. (A.E.).

Received: November 1, 2005
Revised: March 7, 2006
Accepted: June 6, 2006
Published: August 24, 2006

REFERENCES

Alenghat, F.J., and Ingber, D.E. (2002). Mechanotransduction: all signals point to cytoskeleton, matrix, and integrins. Sci. STKE *119*, PE6.

Allingham, J.S., Smith, R., and Rayment, I. (2005). The structural basis of blebbistatin inhibition and specificity for myosin II. Nat. Struct. Mol. Biol. *12*, 378–379.

Andrades, J.A., Santamaria, J.A., Nimni, M.E., and Becerra, J. (2001). Selection and amplification of a bone marrow cell population and its induction to the chondro-osteogenic lineage by rhOP-1: an in vitro and in vivo study. Int. J. Dev. Biol. *45*, 689–693.

Beningo, K.A., Dembo, M., Kaverina, I., Small, J.V., and Wang, Y.L. (2001). Nascent focal adhesions are responsible for the generation of strong propulsive forces in migrating fibroblasts. J. Cell Biol. *153*, 881–888.

Berry, M.F., Engler, A.J., Woo, Y.J., Pirolli, T.J., Bish, L.T., Bell, P., Jayasankar, V., Morine, K.J., Gardner, T.J., Discher, D.E., and Sweeney, H.L. (2006). Mesenchymal stem cell injection after myocardial infarction improves myocardial compliance. Am. J. Physiol. Heart Circ. Physiol. *290*, H2196–H2203.

Bershadsky, A.D., Balaban, N.Q., and Geiger, B. (2003). Adhesion-dependent cell mechanosensitivity. Annu. Rev. Cell Dev. Biol. *19*, 677–695.

Conti, M.A., Even-Ram, S., Liu, C., Yamada, K.M., and Adelstein, R.S. (2004). Defects in cell adhesion and the visceral endoderm following ablation of nonmuscle myosin heavy chain II-A in mice. J. Biol. Chem. *279*, 41263–41266.

Cukierman, E., Pankov, R., Stevens, D.R., and Yamada, K.M. (2001). Taking cell-matrix adhesions to the third dimension. Science *294*, 1708–1712.

Davis, R.L., Weintraub, H., and Lassar, A.B. (1987). Expression of a single transfected cDNA converts fibroblasts to myoblasts. Cell *51*, 987–1000.

Deng, J., Petersen, B.E., Steindler, D.A., Jorgensen, M.L., and Laywell, E.D. (2005). Mesenchymal stem cells spontaneously express neural proteins in culture and are neurogenic after transplantation. Stem Cells *24*, 1054–1064.

Dhawan, J., and Helfman, D.M. (2004). Modulation of acto-myosin contractility in skeletal muscle myoblasts uncouples growth arrest from differentiation. J. Cell Sci. *117*, 3735–3748.

Dinsmore, J., Ratliff, J., Deacon, T., Pakzaban, P., Jacoby, D., Galpern, W., and Isacson, O. (1996). Embryonic stem cells differentiated in vitro as a novel source of cells for transplantation. Cell Transplant. *5*, 131–143.

Discher, D.E., Janmey, P.A., and Wang, Y.-L. (2005). Tissue cells feel and respond to the stiffness of their substrate. Science *310*, 1139–1143.

Engler, A.J., Griffin, M.A., Sen, S., Bonnemann, C.G., Sweeney, H.L., and Discher, D.E. (2004a). Myotubes differentiate optimally on substrates with tissue-like stiffness: pathological implications for soft or stiff microenvironments. J. Cell Biol. *166*, 877–887.

Engler, A.J., Richert, L., Wong, J.Y., Picart, C., and Discher, D.E. (2004b). Surface probe measurements of the elasticity of sectioned tissue, thin gels and polyelectrolyte multilayer films: correlations between substrate stiffness and cell adhesion. Surf. Sci. *570*, 142–154.

Ferrari, G., Cusella-De Angelis, G., Coletta, M., Paolucci, E., Stornaiuolo, A., Cossu, G., and Mavilio, F. (1998). Muscle regeneration by bone marrow-derived myogenic progenitors. Science *279*, 1528–1530.

Flanagan, L.A., Ju, Y.E., Marg, B., Osterfield, M., and Janmey, P.A. (2002). Neurite branching on deformable substrates. Neuroreport *13*, 2411–2415.

Gang, E.J., Jeong, J.A., Hong, S.H., Hwang, S.H., Kim, S.W., Yang, I.H., Ahn, C., Han, H., and Kim, H. (2004). Skeletal myogenic differentiation of mesenchymal stem cells isolated from human umbilical cord blood. Stem Cells *22*, 617–624.

Garcia, A.J., and Reyes, C.D. (2005). Bio-adhesive surfaces to promote osteoblast differentiation and bone formation. J. Dent. Res. *84*, 407–413.

Georges, P.C., Miller, W.J., Meaney, D.F., Sawyer, E., and Janmey, P.A. (2006). Matrices with compliance comparable to that of brain tissue select neuronal over glial growth in mixed cortical cultures. Biophys J. *90*, 3012–3018.

Gilbert, L., He, X., Farmer, P., Rubin, J., Drissi, H., van Wijnen, A.J., Lian, J.B., Stein, G.S., and Nanes, M.S. (2002). Expression of the osteoblast differentiation factor RUNX2 (Cbfa1/AML3/Pebp2alpha A) is inhibited by tumor necrosis factor-alpha. J. Biol. Chem. *277*, 2695–2701.

Griffin, M.A., Sen, S., Sweeney, H.L., and Discher, D.E. (2004). Adhesion-contractile balance in myocyte differentiation. J. Cell Sci. *117*, 5855–5863.

Hinz, B., Celetta, G., Tomasek, J.J., Gabbiani, G., and Chaponnier, C. (2001). Alpha-smooth muscle actin expression upregulates fibroblast contractile activity. Mol. Biol. Cell *12*, 2730–2741.

Hofstetter, C.P., Schwarz, E.J., Hess, D., Widenfalk, J., El Manira, A., Prockop, D.J., and Olson, L. (2002). Marrow stromal cells form guiding strands in the injured spinal cord and promote recovery. Proc. Natl. Acad. Sci. USA *99*, 2199–2204.

Holmbeck, K., Bianco, P., Caterina, J., Yamada, S., Kromer, M., Kuznetsov, S.A., Mankani, M., Robey, P.G., Poole, A.R., Pidoux, I., et al. (1999). MT1-MMP-deficient mice develop dwarfism, osteopenia, arthritis, and connective tissue disease due to inadequate collagen turnover. Cell *99*, 81–92.

Jaiswal, N., Haynesworth, S.E., Caplan, A.I., and Bruder, S.P. (1997). Osteogenic differentiation of purified, culture-expanded human mesenchymal stem cells in vitro. J. Cell. Biochem. *64*, 295–312.

Katagiri, T., Yamaguchi, A., Komaki, M., Abe, E., Takahashi, N., Ikeda, T., Rosen, V., Wozney, J.M., Fujisawa-Sehara, A., and Suda, T. (1994). Bone morphogenetic protein-2 converts the differentiation pathway of C2C12 myoblasts into the osteoblast lineage. J. Cell Biol. *127*, 1755–1766.

Katayama, Y., Battista, M., Kao, W.-M., Hidalgo, A., Peired, A.J., Thomas, S.A., and Frenette, P.S. (2006). Signals from the sympathetic nervous system regulate hematopoietic stem cell egress from bone marrow. Cell *124*, 407–421.

Kim, K.Y., Kovacs, M., Kawamoto, S., Sellers, J.R., and Adelstein, R.S. (2005). Disease-associated mutations and alternative splicing alter the enzymatic and motile activity of nonmuscle myosins II-B and II-C. J. Biol. Chem. *280*, 22769–22775.

Kondo, T., Johnson, S.A., Yoder, M.C., Romand, R., and Hashino, E. (2005). Sonic hedgehog and retinoic acid synergistically promote sensory fate specification from bone marrow-derived pluripotent stem cells. Proc. Natl. Acad. Sci. USA *102*, 4789–4794.

Kong, H.J., Polte, T.R., Alsberg, E., and Mooney, D.J. (2005). FRET measurements of cell-traction forces and nano-scale clustering of adhesion ligands varied by substrate stiffness. Proc. Natl. Acad. Sci. USA *102*, 4300–4305.

Lariviere, R.C., and Julien, J.P. (2004). Functions of intermediate filaments in neuronal development and disease. J. Neurobiol. *58*, 131–148.

Lee, M.S., Lill, M., and Makkar, R.R. (2004). Stem cell transplantation in myocardial infarction. Rev. Cardiovasc. Med. *5*, 82–98.

Limouze, J., Straight, A.F., Mitchison, T.J., and Sellers, J.R. (2004). Specificity of Blebbistatin, an inhibitor of myosin II. J. Muscle Res. Cell Motil. *25*, 337–341.

Lo, C.M., Wang, H.B., Dembo, M., and Wang, Y.L. (2000). Cell movement is guided by the rigidity of the substrate. Biophys. J. *79*, 144–152.

Maitra, A., Arking, D.E., Shivapurkar, N., Ikeda, M., Stastny, V., Kassauei, K., Sui, G., Cutler, D.J., Liu, Y., Brimble, S.N., Noaksson, K., Hyllner, J., Schulz, T.C., Zeng, X., Crook, J., Abraham, S., Colman, A., Sartiny, P., Matsui, S., Carpenter, M., Gazdar, A.F., Rao, M., and Chakravarti, A. (2005). Genomic alterations in cultured human embryonic stem cells. Nat Genet. *37*, 1099–1103.

McBeath, R., Pirone, D.M., Nelson, C.M., Bhadriraju, K., and Chen, C.S. (2004). Cell shape, cytoskeletal tension, and RhoA regulate stem cell lineage commitment. Dev. Cell *6*, 483–495.

Morinobu, M., Ishijima, M., Rittling, S.R., Tsuji, K., Yamamoto, H., Nifuji, A., Denhardt, D.T., and Noda, M. (2003). Osteopontin expression in osteoblasts and osteocytes during bone formation under mechanical stress in the calvarial suture in vivo. J. Bone Miner. Res. *18*, 1706–1715.

Murry, C.E., Soonpaa, M.H., Reinecke, H., Nakajima, H., Nakajima, H.O., Rubart, M., Pasumarthi, K.B.S., Ismail Virag, J., Bartelmez, S.H., Poppa, V., et al. (2004). Haematopoietic stem cells do not transdifferentiate into cardiac myocytes in myocardial infarcts. Nature *428*, 664–668.

Nakagawa, S., Pawelek, P., and Grinnell, F. (1989). Extracellular matrix organization modulates fibroblast growth and growth factor responsiveness. Exp. Cell Res. *182*, 572–582.

Neuhuber, B., Gallo, G., Howard, L., Kostura, L., Mackay, A., and Fischer, I. (2004). Reevaluation of in vitro differentiation protocols for bone marrow stromal cells: disruption of actin cytoskeleton induces rapid morphological changes and mimics neuronal phenotype. J. Neurosci. Res. *77*, 192–204.

Pelham, R.J., and Wang, Y.-L. (1997). Cell locomotion and focal adhesions are regulated by substrate flexibility. Proc. Natl. Acad. Sci. USA *94*, 13661–13665.

Pittenger, M.F., Mackay, A.M., Beck, S.C., Jaiswal, R.K., Douglas, R., Mosca, J.D., Moorman, M.A., Simonetti, D.W., Craig, S., and Marshak, D.R. (1999). Multilineage potential of adult human mesenchymal stem cells. Science *284*, 143–147.

Raisz, L.G. (1999). Physiology and pathophysiology of bone remodeling. Clin. Chem. *45*, 1353–1358.

Rattner, A., Sabido, O., Le, J., Vico, L., Massoubre, C., Frey, J., and Chamson, A. (2000). Mineralization and alkaline phosphatase activity in collagen lattices populated by human osteoblasts. Calcif. Tissue Int. *66*, 35–42.

Roeder, B.A., Kokini, K., Sturgis, J.E., Robinson, J.P., and Voytik-Harbin, S.L. (2002). Tensile mechanical properties of three-dimensional type I collagen extracellular matrices with varied microstructure. J. Biomech. Eng. *124*, 214–222.

Rosania, G.R., Chang, Y.T., Perez, O., Sutherlin, D., Dong, H., Lockhart, D.J., and Schultz, P.G. (2000). Myoseverin, a microtubule-binding molecule with novel cellular effects. Nat. Biotechnol. *18*, 304–308.

Rosenfeld, S.S., Xing, J., Chen, L.Q., and Sweeney, H.L. (2003). Myosin IIb is unconventionally conventional. J. Biol. Chem. *278*, 27449–27455.

Rotsch, C., Jacobson, K., and Radmacher, M. (1999). Dimensional and mechanical dynamics of active and stable edges in motile fibroblasts investigated by using atomic force microscopy. Proc. Natl. Acad. Sci. USA *96*, 921–926.

Rutishauser, U. (1984). Developmental biology of a neural cell adhesion molecule. Nature *310*, 549–554.

Sanger, J., Chowrashi, P., Shaner, N., Spalthoff, S., Wang, J., Freeman, N., and Sanger, J. (2002). Myofibrillogenesis in skeletal muscle cells. Clin. Orthop. Relat. Res. *403S*, S153–S162.

Straight, A.F., Cheung, A., Limouze, J., Chen, I., Westwood, N.J., Sellers, J.R., and Mitchison, T.J. (2003). Dissecting temporal and spatial control of cytokinesis with a myosin II Inhibitor. Science *299*, 1743–1747.

Tamada, M., Sheetz, M.P., and Sawada, Y. (2004). Activation of a signaling cascade by cytoskeleton stretch. Dev. Cell *7*, 709–718.

Tomasek, J.J., Gabbiani, G., Hinz, B., Chaponnier, C., and Brown, R.A. (2002). Myofibroblasts and mechano-regulation of connective tissue remodelling. Nat. Rev. Mol. Cell Biol. *3*, 349–363.

Verkhovsky, A.B., Svitkina, T.M., and Borisy, G.G. (1995). Myosin II filament assemblies in the active lamella of fibroblasts: their morphogenesis and role in the formation of actin filament bundles. J. Cell Biol. *131*, 989–1002.

Wang, N., Tolic-Norrelykke, I.M., Chen, J., Mijailovich, S.M., Butler, J.P., Fredberg, J.J., and Stamenovic, D. (2002). Cell prestress. I. Stiffness and prestress are closely associated in adherent contractile cells. Am. J. Physiol. Cell Physiol. *282*, C606–C616.

Weitzer, G., Milner, D.J., Kim, J.U., Bradley, A., and Capetanaki, Y. (1995). Cytoskeletal control of myogenesis: a desmin null mutation blocks the myogenic pathway during embryonic stem cell differentiation. Dev. Biol. *172*, 422–439.

Wislet-Gendebien, S., Wautier, F., Leprince, P., and Rogister, B. (2005). Astrocytic and neuronal fate of mesenchymal stem cells expressing nestin. Brain Res. Bull. *68*, 95–102.

Woodbury, D., Reynolds, K., and Black, I.B. (2002). Adult bone marrow stromal stem cells express germline, ectodermal, endodermal, and mesodermal genes prior to neurogenesis. J. Neurosci. Res. *69*, 908–917.

Wozniak, M.A., Desai, R., Solski, P.A., Der, C.J., and Keely, P.J. (2003). ROCK-generated contractility regulates breast epithelial cell differentiation in response to the physical properties of a three-dimensional collagen matrix. J. Cell Biol. *163*, 583–595.

Supplemental Tables

Table 1

Gene Description	Symbol	Initial MSC	Expanded MSC	0.1 kPa	1 kPa	11kPa	34kPa	1kPa	11kPa	34kPa
Inhibitors Added								**Bleb**	**Bleb**	**Bleb**
Normalization	**Actin**	**Actin**	**Actin**	**Actin**	**Actin**	**Actin**	**Actin**	**Actin**	**Actin**	**Actin**
ATP-binding cassette G2	ABCG2	0.60	0.51	0.31	0.42	0.58	0.14	0.50	0.62	0.56
Alpha-Fetoprotein	AFP	0.29	0.23	0.18	0.31	0.45	0.04	0.21	0.26	0.25
CD44 Antigen	***CD44***	***0.03***	***0.12***	***0.15***	***0.26***	***0.16***	***0.13***	***0.03***	***0.05***	***0.05***
TAP Binding Protein	TAPBP	0.25	0.30	0.39	0.42	0.52	0.22	0.18	0.32	0.15
CD9 Antigen (p24)	CD9	0.20	0.21	0.64	0.66	0.66	0.18	0.21	0.28	0.38
Integrin, Alpha 1	ITGA1	0.70	0.51	0.20	0.19	0.16	0.34	0.21	0.23	0.27
Integrin, Alpha 2	ITGA2	0.23	0.21	0.43	0.41	0.11	0.15	0.27	0.21	0.19
Integrin, Alpha 3	ITGA3	0.26	0.42	0.22	0.33	0.30	0.25	0.19	0.29	0.23
Integrin, Alpha 4	***ITGA4***	***0.06***	***0.07***	***0.37***	***0.45***	***0.54***	***0.08***	***0.03***	***0.25***	***0.10***
Ig Interleukin 1 Receptor	IL-1R	0.25	0.22	0.50	0.55	0.41	0.09	0.27	0.23	0.16
Interleukin 2 Receptor, Alpha	***IL-2R***	***0.14***	***0.14***	***0.66***	***0.56***	***0.38***	***0.28***	***0.33***	***0.25***	***0.17***
Interleukin 6 Receptor	IL6R	0.33	0.28	0.66	0.69	0.67	0.37	0.40	0.38	0.27
CD34 Antigen	***CD34***	***0.03***	***0.05***	***0.13***	***0.12***	***0.15***	***0.11***	0.03	0.09	0.04
Tyrosine Phospho. Receptor C	***CD45***	***0.12***	***0.20***	***0.25***	***0.26***	***0.26***	***0.18***	***0.15***	***0.15***	***0.11***

Supplemental Table 1: Oligonucleotide array profiles for genes indicating mesenchymal origin. RNA levels were obtained for initially isolated MSCs (passage 4) as well as MSCs expanded in culture (up to passage 12). MSCs from these groups were plated onto 0.1, 1, 11, and 34kPa matrices, grown for 7 days with or without blebbistatin, and also profiled. Raw data was normalized by total actin levels and ranges from 0 (no expression) to 1 (maximal expression). Bold, italicized genes indicate markers that are not generally expressed in the native stem cell population (Pittenger et al., 1999), i.e. – normalized expression in initially isolated MSCs < ~0.15. Note that there is not a dramatic RNA change between initially isolated and expanded MSCs but there are significant expression changes once plated on a compliant gel surface.

Table 2

Media #	Description	Formulation
MSC GM	MSC Growth Media	Low Glucose DMEM + 20% FBS + 1% Penicillin/Streptomycin
MSC MIM	Myoblast Induction Media (MIM)	Low Glucose DMEM + 20% FBS + 1% Penicillin/Streptomycin + 100nM Dexamethasone + 50μM Hydrocortisone
MSC OIM	Osteoblast Induction Media (OIM)	45% Hank's F12 + 45% α-MEM + 10% FBS + 50μM ascorbate-2-phosphate + 10mM β-glycerol phosphate + 100nM Dexamethasone
C2C12 GM FC7 GM	C2C12 Growth Media (GM)	78% High Glucose DMEM + 20% FBS + 1% Chicken Embryo Extract + 1% Penicillin/Streptomycin
hFOB GM	hFOB Growth Media (GM)	45% Hank's F12 + 45% DMEM + 10% FBS

Supplemental Table 2: Growth conditions for all cell types utilized. All MSC cultures use MSC GM for all experiments, except when noted.

Table 3

Gene Description	Symbol	Lineage Marker	0.1 kPa MSC	1 kPa MSC	11 kPa MSC	34 kPa MSC	1 kPa MSC	11 kPa MSC	34 kPa MSC	11 kPa MSC	34 kPa MSC
Inhibitors Added							**Bleb**	**Bleb**	**Bleb**		
(Normalization)			**Actin, MSC**	**Actin, MSC**	**Actin, MSC**	**Actin, MSC**	**Actin, MSC**	**Actin, MSC**	**Actin, MSC**	**Actin, C2C12**	**Actin, hFOB**
Microtubule-Assoc Prot. Tau	MAPT	N	5.56	7.63	3.70	1.51	1.45	0.88	1.02		
Tau Tubulin Kinase 1	TTBK1	N	5.23	7.28	4.40	1.89	1.62	1.38	1.09		
Tau Tubulin Kinase 2	TTBK2	N	3.56	4.89	3.50	1.74	1.29	0.97	0.93		
Tubulin, Alpha 3	TUBA3	N	1.97	1.25	0.94	0.64	1.11	0.55	0.46		
Tubulin, Beta 1	TUBB1	N	8.41	8.88	5.13	1.50	3.63	1.85	1.26		
Tubulin, Beta 3	TUBB3	N	5.70	3.73	1.49	1.17	1.62	1.02	0.86		
Tubulin, Beta 4	TUBB4	N	8.55	9.67	3.98	0.79	3.42	1.46	0.94		
Glial Der. Neurotrophic Fctr	GDNF	N	9.88	9.67	2.65	1.15	2.18	1.38	1.20		
GDNF Receptor Alpha 1	GFRA1	N	5.14	5.29	2.01	1.16	1.45	1.15	1.02		
N-Cadherin	CDH2	N	2.19	4.70	6.38	1.62	1.52	1.58	1.14		
TNF Receptor Member 5	CD40	N	3.73	6.51	3.72	2.10	1.82	1.39	1.24		
TNF Receptor, Member 6	FAS	N	4.41	6.62	4.21	2.07	2.38	1.71	1.01		
Brain-Der. Neurotrophic Fctr	BDNF	N	4.27	5.72	1.14	1.35	2.52	1.09	1.18		
Neurofilament Light Chain	NEFL	N	3.62	4.13	2.00	1.23	1.97	0.93	0.86		
Internexin Neuronal IFα	INA	N	6.53	6.17	2.52	1.33	2.13	0.64	0.79		
Nerve Growth Factor Beta	NGF	N	4.48	4.46	2.33	1.75	1.20	0.66	0.94		
Neuregulin 1	NRG1	N	4.38	4.67	2.97	1.58	2.12	1.15	0.95		
Signal Activator of Transcrpt. 3	STAT3	N	4.57	5.41	2.07	1.64	1.56	0.73	0.98		
Nestin	NES	N	3.30	4.25	1.38	2.22	1.27	0.44	0.96		
Neural CAM 1	NCAM1	N	7.57	4.55	2.58	2.45	2.33	1.58	1.73		
Integrin, Beta 3	ITGB3	N	0.59	0.72	0.58	0.56	0.78	0.59	0.55		
Paired Box Gene 3	PAX3	M	2.45	2.56	6.96	1.60	0.90	2.49	0.97	0.56	
Paired Box Gene 7	PAX7	M	3.56	3.01	9.40	2.14	0.83	2.60	1.58	0.59	
Myogenic Factor 3	MYOD1	M	2.09	2.20	6.15	1.64	1.14	2.08	1.02	0.58	
Myogenic Factor 4	MYOG	M	2.49	3.48	11.63	1.96	1.15	2.68	0.94	0.59	
Myogenic Factor 5	MYF5	M	2.08	2.82	6.17	1.90	0.71	1.87	1.02	0.65	
Myogenic Factor 6	MYF6	M	2.26	3.50	7.02	2.33	0.77	1.61	1.25	0.76	
Mesenchyme Homeobox 2	MEOX2	M	5.52	6.08	8.81	2.44	1.36	2.08	0.97	0.46	
Forkhead Box K1	FOXK1	M	2.45	2.55	5.12	2.15	1.36	1.97	1.04	0.59	
Myostatin	GDF8	M	3.94	3.21	6.09	2.02	1.16	2.40	1.04	0.67	
MADS Enhancer Factor 2A	MEF2A	M	6.30	3.68	6.23	2.37	1.42	2.52	1.64	0.62	
MADS Enhancer Factor 2B	MEF2B	M	2.83	1.75	7.17	1.89	1.05	2.62	1.01	0.53	
MADS Enhancer Factor 2C	MEF2C	M	2.44	1.69	9.16	2.38	1.03	2.68	1.06	0.57	
MADS Enhancer Factor 2D	MEF2D	M	1.24	1.00	4.29	1.70	0.93	1.37	1.08	0.57	
Growth Fctr Bound Rcptr. 2	GRB2	M	2.20	2.41	6.28	2.63	1.04	2.27	1.16	0.64	
Desmin	DES	M	2.18	2.34	5.13	2.03	1.08	2.83	1.11	0.46	
Msh Homeobox Homolog 1	MSX1	M	1.48	1.57	4.33	1.65	0.98	1.77	0.94	0.63	
Msh Homeobox Homolog 2	MSX2	M	0.70	0.71	1.58	1.08	0.82	1.15	0.81	1.00	
Ladybird H-box Homolog 1	LBX1	M	1.94	1.99	5.08	1.97	0.84	2.03	0.94	0.66	
Nebulin-Rel. Anchoring Prot	NRAP	M	2.47	1.87	8.15	3.52	0.91	2.35	1.66	0.58	
Myotilin	TTID	M	2.08	1.13	5.09	1.58	0.92	2.04	1.04	0.67	
Titin	TTN	M	2.30	1.19	7.40	4.07	0.92	2.51	1.10	0.65	
M-Cadherin	CDH15	M	2.79	2.29	8.46	2.73	1.14	1.93	1.34	0.75	
Integrin, Beta 1D	ITGB1D	M	0.35	0.40	1.22	0.85	0.82	1.04	0.85	0.54	
Integrin, Alpha 7	ITGA7	M	0.28	0.41	1.69	1.03	0.98	1.24	0.96	0.55	
Core Binding Factor Alpha 1	CBFA1	O	0.93	1.31	2.16	2.89	0.93	0.90	1.42		0.37
Cadherin 11, Type 2	CDH11	O	0.56	0.54	0.90	1.55	0.63	0.88	1.23		0.69
Osteopontin	SPP1	O	1.25	0.83	1.91	2.61	0.83	1.04	1.23		0.36
Tuftelin Interact'g Protein 11	TFIP11	O	1.26	0.79	2.87	2.62	0.04	0.70	1.26		0.48
Twist Homolog 1	TWIST1	O	1.47	1.06	2.16	3.73	0.98	1.08	1.36		0.43
Twist Homolog 2	TWIST2	O	1.95	1.96	4.94	5.53	0.97	1.19	2.56		0.49
Sex Det. Region Y-box 9	SOX9	O	1.92	2.64	2.67	2.69	1.48	1.27	1.35		0.32
SMAD, Mothers Against DPP 1	SMAD1	O	1.74	2.39	3.26	7.23	1.36	1.37	2.89		0.81
SMAD, Mothers Against DPP 2	SMAD2	O	2.17	2.38	3.11	3.25	1.08	1.41	1.47		0.36
SMAD, Mothers Against DPP 3	SMAD3	O	2.17	2.73	2.89	2.85	0.96	1.01	1.13		0.34
SMAD, Mothers Against DPP 4	SMAD4	O	2.06	1.92	3.94	2.68	0.91	1.10	1.80		0.44
SMAD, Mothers Against DPP 5	SMAD5	O	2.53	2.50	4.11	5.85	0.97	1.81	2.13		0.43
SMAD, Mothers Against DPP 6	SMAD6	O	3.73	5.39	4.94	6.80	1.06	1.45	2.89		0.42
SMAD, Mothers Against DPP 7	SMAD7	O	2.53	3.96	2.53	6.06	0.99	1.24	3.43		0.50
SMAD, Mothers Against DPP 9	SMAD9	O	2.61	3.49	2.51	2.89	0.87	1.13	2.52		0.36

Vitamin D receptor	VDR	O	2.70	3.32	3.32	3.24	1.18	1.42	1.99		0.42
Osteocalcin	BGLAP	O	3.36	5.13	4.99	12.03	0.92	1.30	2.94		0.48
Bone Morpho. Protein 1	BMP1	O	3.81	5.43	4.20	3.46	1.10	1.84	3.07		0.41
Bone Morpho. Protein 2	BMP2	O	2.23	3.29	2.50	2.78	1.09	1.88	2.57		0.43
Bone Morpho. Protein 3	BMP3	O	3.34	5.08	3.05	4.09	1.02	2.09	2.68		0.44
Bone Morpho. Protein 4	BMP4	O	2.91	5.61	3.81	3.38	1.25	1.99	2.96		0.54
Bone Morpho. Protein 5	BMP5	O	2.67	5.38	2.79	3.78	1.19	1.79	2.93		0.63
Bone Morpho. Protein 6	BMP6	O	1.76	3.53	1.20	2.41	0.89	1.23	1.75		0.54
Bone Morpho. Protein 7	BMP7	O	1.91	2.89	2.06	2.09	0.89	1.09	1.87		0.45
Bone Morpho. Protein 8B	BMP8B	O	1.62	3.27	2.11	2.15	0.96	1.62	1.52		0.49
Bone Morpho. Protein Rcptr 1A	BMPR1A	O	1.72	2.86	1.60	1.71	0.93	1.13	1.33		0.64
Matrix Gla Protein	MGP	O	1.91	2.54	1.63	1.46	1.43	1.02	1.67		0.68
Collagen, Type 1, Alpha 1	COL1A1	O	0.78	0.96	0.51	1.09	0.99	0.78	1.08		1.00
Collagen, Type 1, Alpha 2	COL1A2	O	0.69	0.89	0.42	1.00	0.99	1.22	1.32		1.00
Collagen, Type 3, Alpha 1	COL3A1	O	3.67	4.88	2.32	2.35	1.20	1.61	2.13		0.71

Supplemental Table 3: Expression of neurogenic (N), myogenic (M), and osteogenic (O) genes in MSCs cultured on 0.1, 1, 11, and 34 kPa matrices (with and without blebbistatin treatment) was assayed using an oligonucleotide array. Data was normalized to actin levels and compared to gene expression of low (4) passage MSCs ([MSC on specific gel]/MSC). Values displayed represent relative fold changes from initially isolated MSCs. mRNA expression for MSCs cultured on 11 and 34 kPa matrices (with and without blebbistatin treatment) was also expressed as a fraction of mRNA expression in C2C12 myoblasts or hFOB osteoblasts for those indicated genes, and range between 0 (i.e.- no expression) and 1 (i.e. – full expression at positive control cell levels).

Table 4

Gene Description	**Symbol**	**Lineage Marker**	**0.1 kPa MSC**	**1 kPa MSC**	**11 kPa MSC**	**34 kPa MSC**	**1 kPa MSC**	**11 kPa MSC**	**34 kPa MSC**
Inhibitors Added							**Bleb**	**Bleb**	**Bleb**
(Normalization)			**Actin**	**Actin**	**Actin**	**Actin**	**Actin**	**Actin**	**Actin**
Myosin IA	MYO1A	Myo	0.52	0.69	1.38	1.19	0.69	1.07	0.90
Myosin IIIB	MYO3B	Myo	1.80	1.79	3.88	2.42	0.48	0.62	0.51
Myosin VB	MYO5B	Myo	0.40	0.50	1.46	1.32	0.71	1.25	0.87
Myosin IXa	MYO9A	Myo	1.52	1.72	2.57	1.69	0.51	0.63	0.47
Myosin VI	MYO6	Myo	1.53	1.67	2.28	1.83	0.00	0.02	0.03
Myosin Light Chain III	MYL6	Myo	0.72	0.67	0.92	1.01	0.69	0.97	0.74
Myosin Heavy Chain IIa	MHC2a	Myo	1.15	1.92	4.03	3.01	0.05	0.22	0.12
Sk. Muscle Myosin Heavy III	MYH3	Myo	3.80	3.93	4.69	2.84	0.46	0.75	0.56
Non-Muscle Myosin IIA	NMM2A	Myo	0.63	0.70	1.12	1.01	0.21	0.29	0.27
Non-Muscle Myosin IIB	NMM2B	Myo	4.06	3.81	6.69	2.45	0.02	0.08	0.01
Non-Muscle Myosin IIC	NMM2C	Myo	2.17	2.24	2.95	1.96	0.01	0.06	0.00
hMyosin Light Chain IIB	HML2B	Myo	1.20	1.37	2.53	1.73	0.54	0.65	0.56
Talin 1	TLN1	A	0.82	0.86	1.02	1.21	0.54	0.73	0.80
Filamin C, Gamma	FLNC	A	0.84	0.82	1.04	1.26	0.66	0.98	0.78
Paxillin	PXN	A	1.31	1.24	1.46	1.68	0.42	0.50	0.46
Vinculin	VCL	A	4.31	5.53	5.11	4.39	0.38	0.37	0.32
Laminin, Alpha 2	LAMA2	A	0.98	1.10	1.40	1.09	0.28	0.28	0.29
Actinin, Alpha 1	ACTN1	A	0.57	0.65	1.25	1.06	0.25	0.52	0.37
PTK2 Protein Tyrosine Kinase	PTK2	S	0.81	0.82	1.20	1.25	0.38	0.61	0.43
Ras Homolog A	RHOA	S	0.73	0.86	1.25	1.14	0.28	0.45	0.37
Ras-C3 Botulinum Substrate 1	RAC1	S	2.64	2.12	1.17	2.82	0.45	0.29	0.54
Cell Division Cycle 42	CDC42	S	1.48	1.71	1.23	1.56	0.50	0.26	0.49
Rho-Assoc. Coil-Coil Kinase 1	ROCK1	S	1.17	0.81	1.03	2.15	0.26	0.41	0.59
Diaphanous Homolog 2	DIAPH2	S	2.99	3.25	4.64	1.79	0.31	0.35	0.29
Striated Muscle Activator-Rho	STARS	S	1.61	1.56	3.62	0.95	0.69	1.07	0.90

Supplemental Table 4: RNA levels for myosin (Myo), adhesion (A), and cell signaling (S) genes were obtained for MSCs plated onto 0.1, 1, 11, and 34kPa matrices (with or without blebbistatin) for 7 days. Raw data was normalized by total actin levels and ranges from 0 (no expression) to ~1 (maximal expression).

Supplemental Methods and Text

Creep-test Micropipette Aspiration:
Micropipettes were forged using a deFonbrune-type microforge (Vibratome, St. Louis, MO) to a radius of 2-3 μm with an approximately 25^o pipette curvature so when mounted in micromanipulators (Nirishige; Japan) at an angle similar to the micropipette's curvature, the end of the pipette was flush with the cell edge (Supplemental Figure 1A). A step pressure drop was imposed on the cell membrane, causing the membrane projection, L, to aspirate into the pipette as a function of time, t, pressure drop ΔP and pipette radius, R, as governed by Sato and coworkers (Sato et al., 1990) viscoelastic half-space model:

$$L(t) = \frac{3R\Delta P}{\pi\kappa}\left[1 - \frac{\mu'}{\kappa + \mu'}\exp\left(\frac{-t}{\tau}\right)\right] \qquad \text{(Eq.S0)}$$

Images of the projection length were taken every 2 seconds in brightfield on a TE300 inverted Nikon microscope and cascade CCD camera (Photometrics), which allowed accurate fitting of the parameters κ, μ', and τ to the data to determine each membrane's elastic and viscous moduli.

Traction Force Measurements:
Displacement fields generated from cell tractions (eg.(Wang et al., 2002) were mapped from embedded beads within a soft substratum. Briefly, traction force microscopy uses bead displacements between images with and without the adherent cell to assemble a displacement field and determine Green's strain function given known material properties of the substratum (elastic modulus, poisson's ratio, etc). The traction field was used to obtain the cell prestress, i.e. – the net tensile force through the cell's cross-sectional area (Wang et al., 2002).

Getting Physical: Matrix Strain *versus* Cellular Strain suggests an Effective Energy Description for Lineage Specification

As a function of matrix stiffness, the two differentiated cell types, the C2C12-myoblasts and hFOB-osteoblasts exhibit similar slopes for (κ/E) – though the intercepts are distinct (Fig. 7B, bottom). By using the prestress results (Fig. 7B, top), these two differentiated cell types have the same slope for (κ/σ) ($\approx$ 0.2) that has been reported for highly contractile, smooth muscle cells as assayed by a very different technique (Wang et al., 2002). On the other hand, MSCs appear more mechano-sensitive, with twice the slope for (κ/E) and (κ/σ). This increased mechano-sensitivity leads to a self-consistent crossover: on myogenic gels (11 kPa), MSCs and C2C12s have similar κ whereas on osteogenic gels (34 kPa), MSCs and hFOBs have similar κ. Despite the revealing difference, the inside-outside relationship between intracellular strains, ε_{in} (= σ / κ), and the mean extracellular strain, ε_{out} (= τ / E), fits a universal power-law for all cell types (Fig. 7, inset). One can perhaps equate such a strain comparison to comparisons of intracellular ion concentrations to extracellular ion concentrations (eg. $[Ca^{++}]_{in}$ versus $[Ca^{++}]_{out}$, etc.). The inverse relationship between intracellular strains and extracellular strains here reveals that, on stiff matrices, cell strains are large while matrix strains are small. In contrast, on soft matrices, cell strains are small and matrix strains are large. The strain thus transfers from outside to in with increasing matrix stiffness, presumably activating different pathways at different strains. However, the power-law (of form $\varepsilon_{in} = B\,\varepsilon_{out}^{b}$) found for all cell types implicates a common mechanism, which is consistent with a central contractile role in matrix-sensing and response based on non-muscle myosin II (Fig. 7, bottom curves).

Just as Nernst-type electrochemical equations formalize electrophysiology and help clarify the summed contributions of channel permeabilities, we suggest that our findings here might also be formalized in a simple thermodynamic model to fit our differentiation results of Figure 3C. In electrophysiology, the net negative charge of intracellular macro-ions (DNA, protein, etc) is key, whereas here the net contractile stress of intracellular myosins (NMMII's especially) is key. Instead of the channel activity at membranes, the chemomechanical energetics here localize to membrane-matrix adhesions and balance the contractile energetics of the cell. We assume two key states for the limiting association of a key, lineage-specific component 'X_i' which associates with apparent affinity K in or near the focal adhesions and

obeys a molecular partition function, ξ, that cooperatively links to collagen (*coll*) with a Hill coefficient *m* to give:

$$\xi = 1 + [(K/E)\ coll]^{m} \qquad \text{(Eq. S1)}$$

In terms of energetics, $K \sim \exp(-\Delta G/k_bT)$ and the matrix modulus $E \sim A \exp(\kappa x^2/k_bT)$. Additionally, κ is the relevant stiffness of matrix/membrane/adhesions and *x* is a strain. If κx^2 is small, $E \sim A\ [1 + (\kappa x^2/k_bT)]$ which implies that κ is linear in *E*, as shown in Figure 5B for cortical stiffness.

We assume that the fraction of unbound X_i matters most for lineage specificity: $\theta' = 1 - [\ \partial \ln(\xi) / \partial \ln(coll)] = 1 / \xi$. This is the free and diffusible fraction of X_i (not associated with collagen) that has the strongest effect. With *N* as the total number of species X_i, the total unbound portion of this species is $\Theta' = N\theta' = N/\xi$, which gives a chemomechanical potential for $N = constant$ as:

$$G_{chem} = -k_bT \ln(N / \xi) = constant\ - k_bT \ln [\ 1 + [(K/E)\ coll]^{m}\ ]^{-1} \qquad \text{(Eq. S2)}$$

The free energy depends additionally on the global prestress, σ, assumed to act throughout the cell volume *V* as a global regulator of differentiation. Coupled to this, an increase in free concentration of the local, transducing activator/effector links cooperatively to collagen (with Hill coefficient *m* and affinity *K*) and to matrix stiffness (*E*) to yield $G_{tot} = G_{chem} + \sigma V$. The net result is a lineage commitment probability given by:

$$P_{lineage}(E) = a_0 + a_1\ exp(-\sigma V / k_B T_{eff}) \left[\frac{E^m}{E^m + K^m coll^m} \right] \qquad \text{(Eqn. S3)}$$

The effective thermal energy k_BT_{eff} in the exponential should relate more to cytoskeletal stochastics than temperature (Lau et al., 2003; Le Goff et al., 2002). In the limit of rigid substrates with high tensions (σ), isometric pulling on adhesions will limit MSC specification, as seen here (Fig. 3C and 4A, B).

Equation S3 fits the three differentiation peaks of Fig. 3C (at $E^* \approx 0.3$ kPa, 10 kPa, 30 kPa) with best fit values for the key parameters *K*, *m*, and T_{eff} determined for peaks at $E^* \approx 0.3$ kPa, 10 kPa, 30 kPa as (*K*, *m*, and T_{eff}): $(2.8\cdot10^{-4}, 2.4, 9.5\cdot10^{-8})$, $(2.2\cdot10^{-2}, 4.8, 3.4\cdot10^{-7})$ $(4.2\cdot10^{-2}, 8.1, 1.3\cdot10^{-6})$. . All of these parameters increase with increasing E^*, and the cooperativity *m* notably rises from about 2 to 8 (recall that oxygen binds hemoglobin with $m \approx 4$), suggesting the progressive formation of large signaling complexes, consistent with growing adhesions (Fig. 6A), and increased coupling to the microenvironment.

Supplemental References

Lau, A.W., et al., *Microrheology, stress fluctuations, and active behavior of living cells.* Phys Rev Lett, 2003. **91**(19): p. 198101.

Le Goff, L., F. Amblard, and E.M. Furst, *Motor-driven dynamics in actin-myosin networks.* Phys Rev Lett, 2002. **88**(1): p. 018101

Paszek, M. J., Zahir, N., Johnson, K. R., Lakins, J. N., Rozenberg, G. I., Gefen, A., Reinhart-King, C. A., Margulies, S. S., Dembo, M., Boettiger, D.*, et al.* (2005). Tensional homeostasis and the malignant phenotype. Cancer Cell *8*, 241-254.

Sato, M., Theret, D. P., Wheeler, L. T., Ohshima, N., and Nerem, R. M. (1990). Application of the micropipette technique to the measurement of cultured porcine aortic endothelial cell viscoelastic properties. J Biomech Eng *112*, 263-268

Supplemental Figures

Supplemental Figure 1: Myogenic Lineage Commitment Stops Short of Skeletal Muscle Protein Expression. (**A**) Like MSCs spreading on soft matrices and becoming branched, MSCs will both actively spread and elongate with time while they stop short of full specification as (**B**) skeletal muscle myosin heavy chain-stained MSCs show minimal expression after 7 days, regardless of matrix stiffness or media stimulus (not shown). Myoblasts, however, show 5- to 10-fold higher expression regardless of matrix mechanics**.**

Supplemental Figure 2: MyoD Regulation by Blebbistatin. MSCs, plated on 11 kPa gels for 24 hours prior to blebbistatin addition (closed arrow), were able to maintain their spindle morphology (open points). MyoD expression (closed points) was never observed in MSCs continually treated with blebbistatin. However, when blebbistatin was subsequently washed-out after a 72 hour exposure (open arrow), MyoD fluorescence recovered on a similar time-scale to the initial commitment observed in untreated cells.

Supplemental Figure 3: Cell Spreading on Ultra-thin Polyacrylamide Gel. Cells contract their matrices up to 1-3 microns (Wang et al., 2002) so that on thin, soft gels (h ~ 500 nm) attached to glass, cells are expected to 'feel' a matrix that is effectively stiffer than the cast gel. The result is an enhanced spreading of the cells, which allows mapping the spread area on thin gels to that for thick gels and determination of an 'apparent' gel modulus (inset). The dark gray shaded region represents the $E_{apparent}$, given experimental uncertainties.

Supplemental Figure 4: Membrane Cortex Viscoelasticity. (**A**) For micropipette aspiration, a curved pipette was brought into contact with the side of an adherent cell, a step pressure drop aspirated a portion of membrane, and the projection length extending over time is fit to a viscoelastic model, Eq. 3. (**B**) Sample aspiration data of 5 cells from a single matrix stiffness shows the range of variability. Inset images illustrate this phenomenon, with arrows indicating the membrane cap. Scale bar is 5 μm.

Figure S1

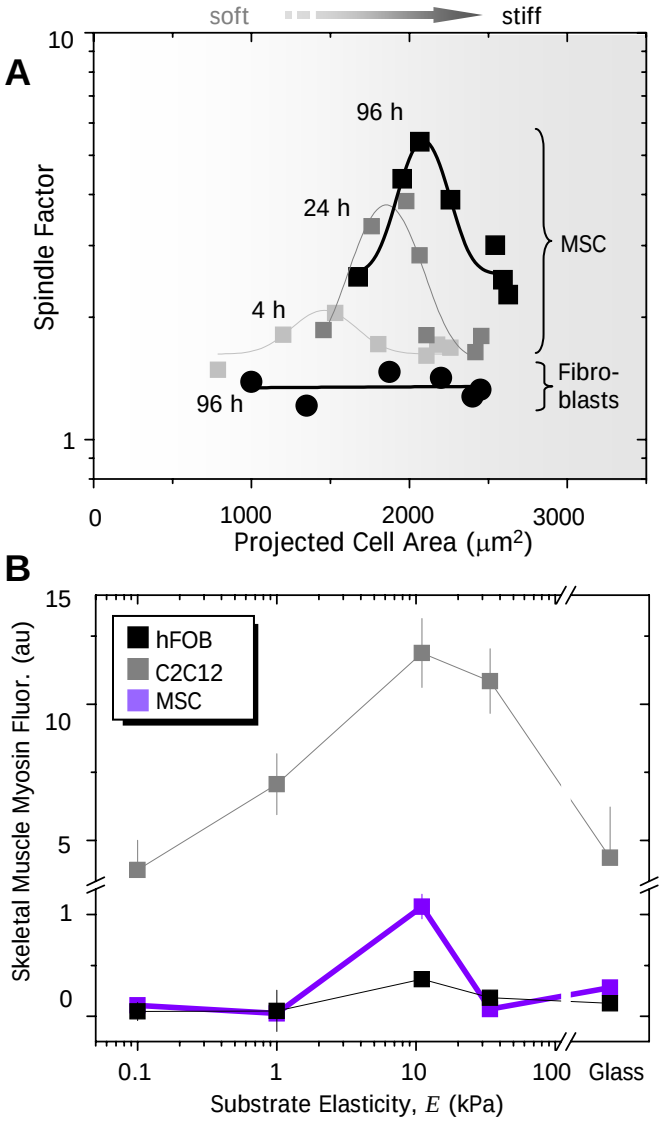
soft
stiff
A
10
1
Spindle Factor
96 h
24 h
4 h
96 h
MSC
Fibro-
blasts
0
1000
2000
3000
Projected Cell Area (μm²)
B
15
10
5
1
0
Skeletal Muscle Myosin Fluor. (au)
hFOB
C2C12
MSC
0.1
1
10
100
Glass
Substrate Elasticity, E (kPa)

Figure S2

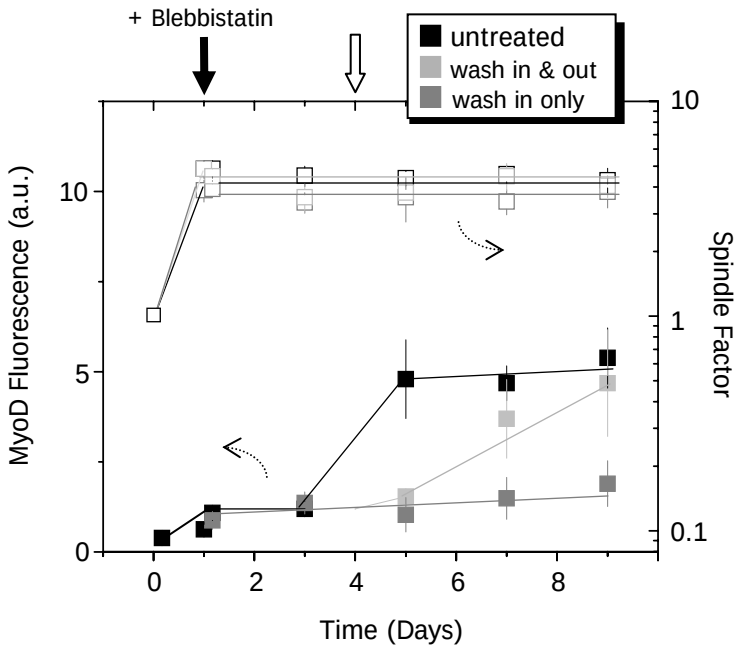
+ Blebbistatin
untreated
wash in & out
wash in only
MyoD Fluorescence (a.u.)
Spindle Factor
Time (Days)
0
5
10
0.1
1
10
0
2
4
6
8

Figure S3

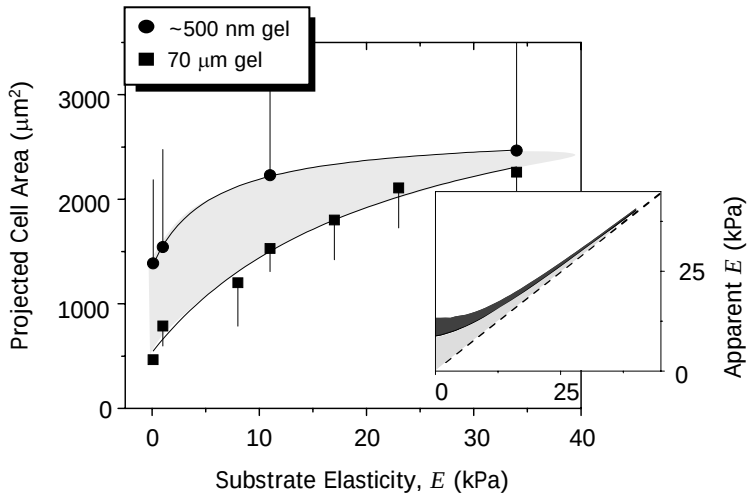

Figure S4